Chapter 6

Improvement of Abel inversion using VTEC data

This chapter deals with the improvement of the classical Abel inversion through two main issues:

1. Inclusion of horizontal information of ionospheric electron density distribution to overcome the assumption of spherical symmetry.
2. Estimation of the contribution of electron density above the LEO GPS satellite.

To show this improvement, this chapter details these points before describing the implementation of the model used to process the occultations. Afterwards, results with several LEOs are shown quantifying this improvement. The data used consists in simulated data as well as several real data sets corresponding to different scenarios.

6.1 Including VTEC information

As explained in Chapter 4, the classical approach of the Abel inversion assumes spherical symmetry in the locality of the occultation, which states that the electron content varies in height, but not horizontally. This implies, in particular, a constant VTEC in the occultation region. Nevertheless, since the ionosphere shows either vertical and horizontal variation despite the typical short time span of few minutes during the occultation, this assumption may not be realistic in many circumstances, thus causing a mismodelling. A particular example of the variability can be seen in Figure 6.1, where it is depicted a VTEC map of the Southeastern Asia and Oceania. This map shows a particular example near the geomagnetic equator (in the region of the southern equatorial anomaly), where non-linear variations of VTEC can reach 50 TECUs or even more in Solar Maximum or large geomagnetic storm conditions.

In particular, strong gradients (i.e. high spatial variability) of VTEC are expected to be higher in the following situations:

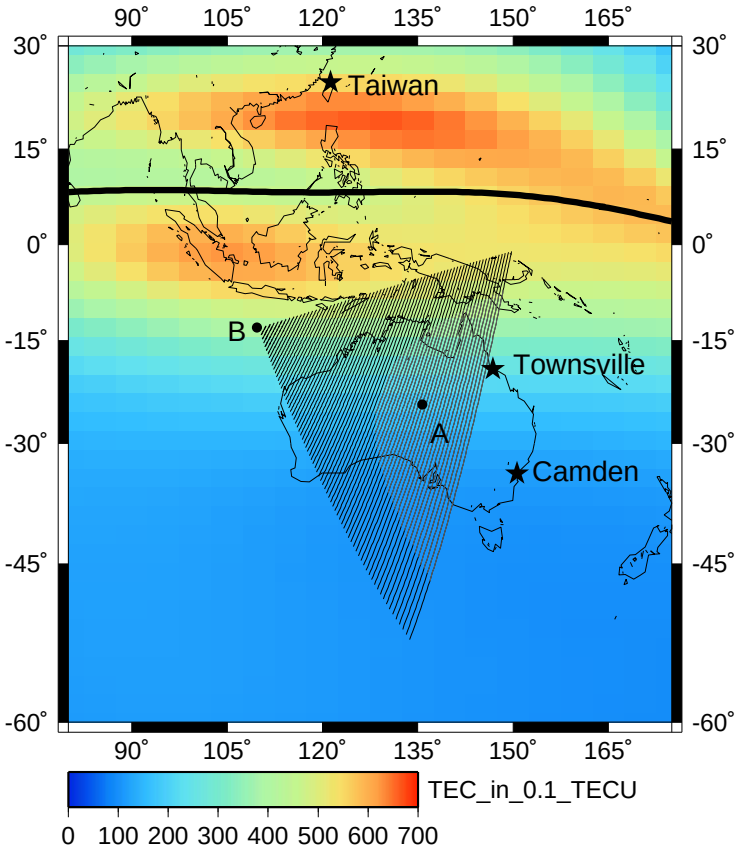

Figure 6.1: Presence of VTEC gradients during an occultation. The diagonal thin lines represent the typical footprint (i.e. projection on the Earth surface) of the rays linking the LEO and GPS satellite (which are assumed to be straight-lines). Only the portion of rays under the LEO orbit (in this case the GPS/MET, with nominal orbit of 750km) is depicted. Black and grey lines are the portion of rays above and under 400km respectively. The points A and B are the geographical coordinates of the tangent points (T) corresponding to the rays which height of the tangent point are 300km and 700km respectively. Note the presence of the Appleton-Hartree anomalies near the geomagnetic equator (black thick line).

1. Since the Sun is the main source of ionisation, the **day/night terminators** (i.e. dawn and dusk periods) cause gradients of VTEC.

2. The presence of the Appleton-Hartree anomalies, in **regions near the geomagnetic equator** induce large variations in the distribution of the electron density. Note, for instance, that in the vicinity of these Equatorial Anomalies depicted in Figure 6.1 variations of 50TECUs or even more can be induced.

3. Large geomagnetic storms, that cause **Ionospheric disturbances**.

Note that, as mentioned in section 4.1.2, the mismodelling due to spherical symmetry is increased as the rays traverse the lowest layers of the ionosphere (i.e. E layer). This is due to two main causes:

1. Since the Abel inversion algorithm is a recursive method in which the upper layers are solved for before the lower layers, the accumulative errors on the former will greatly affect the latter.

2. The rays are longer in the lower layers (see Figure 6.1), therefore the occurrence of horizontal gradients cause a more important effect than in the upper layers.

This chapter deals on how the information about horizontal variability of the ionosphere, in particular information about the VTEC, can be included in the Abel inversion scheme in order to overcome the spherical symmetry assumption. The choice of the VTEC is justified since it follows similar variation than the electron density. In particular one can focus in the relationship between the VTEC and the NmF2, known as *slab thickness* (τ) defined as:

$$\tau = \frac{VTEC}{NmF2} \tag{6.1}$$

The interpretation of the slab thickness (which can be expressed in meters) is the height width of an imaginary ionosphere with constant electron density equal to the NmF2 and VTEC equal to the actual ionosphere. Several works have shown that, except periods of storms, day/dusk periods or other ionospheric irregularities, the slab thickness tends to show a constant behavior during day and night time ([Davies, 1990],[Breed and Goodwin, 1998]), which implies a corresponding direct proportionality between the VTEC and the NmF2.

Therefore, as a first approach, it is plausible to expect similar variations of VTEC and electron density. Following this approach, VTEC maps can be useful to overcome the assumption of spherical symmetry. To take advantage of this information in the Abel inversion scheme, a *separability assumption* between the VTEC and a Shape Function (or Normalized electron density profile) was introduced in [Hernandez-Pajares et al., 2000], therefore:

$$N_e(\lambda, \phi, h) = VTEC(\lambda, \phi) \cdot F(h) \tag{6.2}$$

where λ can be either local time or latitude (depending on the chosen reference frame), ϕ is latitude and h is height. The $VTEC(\lambda, \phi)$ provides with the horizontal gradients of integrated electron density. The Shape Function F (which has units of m^{-1}, it is the unknown to solve) will describe the vertical distribution of electron density. Note that with this shape function, the N_e does not depend only on height anymore, a horizontal variation has been introduced to compute the N_e profile.

Variability of Shape Function and Electron density profiles

This subsection will show, by means of using the IRI model, that is more realistic to assume that the shape function depends only on height and to use the VTEC information to account for the horizontal variation, rather than considering spherical symmetry directly in the electron density function.

For this study, the orbits of the GPSMET and GPS satellites for the day 1995 October 18th (day of year 291) have been used, thus giving the true geometry involved in the occultations for this epoch. The ionosphere was simulated using the IRI model according to this geometry. A total number of 209 occultations were processed.

Let us focus again on the map of Figure 6.1 and the points A and B. This section will check the difference between the vertical profiles (taken from the IRI model) at these points. Note that in this section no Abel inversion is performed, only vertical profiles computed with IRI are compared. To quantify these differences two parameters are given:

1. The percentual difference expressed as the **relative RMS percentage of the whole profile**, defined as:

$$RMS_{profile} = \frac{100}{mean\ value} \cdot \sqrt{\frac{\sum(\zeta_A(h) - \zeta_B(h))^2}{n}} \tag{6.3}$$

   where $\zeta_A(h)$ is either the electron density profile or shape function (i.e. electron density profile divided by the VTEC) at point A and $\zeta_B(h)$ for point B. The number of points of the profile is noted by n and the $mean\ value$ is the average value of the profile.

2. The **difference of the peak**, defined as:

$$Difference\ peak = \frac{\zeta_{A,max} - \zeta_{B,max}}{\zeta_{B,max}} \times 100 \tag{6.4}$$

The reason for giving two comparisons is due to errors caused by shift heights, seen in Section 5.3.2. Even if the shape of the two profiles (and in particular the value of the peak) is similar, if a height displacement exists between them, the difference expressed as the RMS of the whole profile can be large.

Figure 6.2 shows the electron density profiles (right panel) and shape functions (left panel) for an occultation in which the A and B points are close (46km).

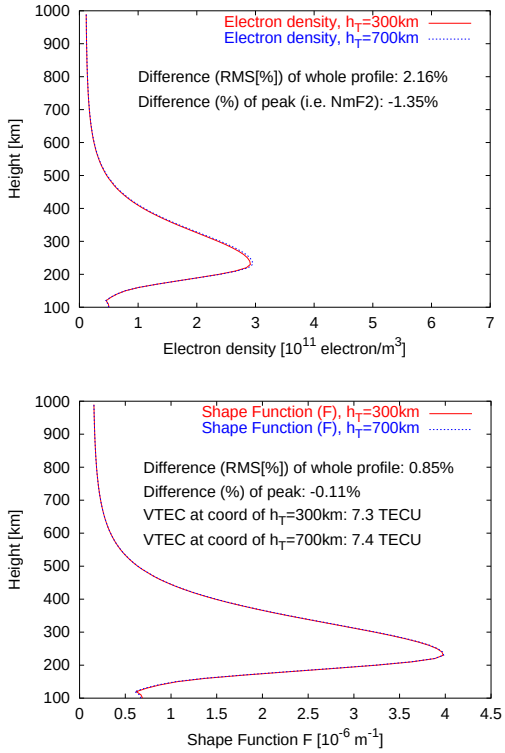

Figure 6.2: Electron density profiles and shape functions for an occultation with points A($157.5^oE59.3^oN$)/B($158.2^oE59.5^oN$) separated 46km. Note that the profiles, from the IRI model, are practically superimposed. The inversion corresponds to an occultation of the PRN09 at the epoch 1995 October 18th, 22hUT

Since in this case the points are close, the differences in both cases are small, even unnoticeable, specially in the case of the Shape function (F). Nevertheless if these points happen to be not so closer, the differences increase. Figure 6.3 depicts the comparison of profiles for an occultation in which the A and B points are further (943 km). Note that, for the Shape function, the values of profile are similar but for a shift height. This increases the RMS of the whole profile (although the peak difference in both close and far cases are similar).

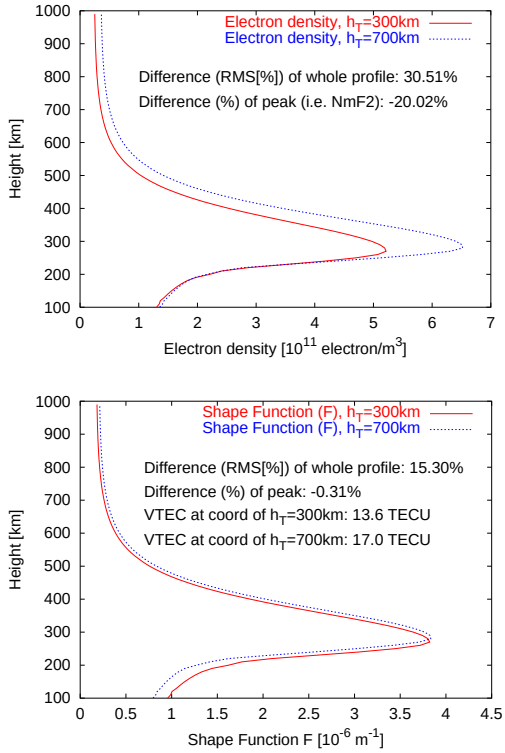

Figure 6.3: Electron density profiles and shape functions for an occultation with points A($79.2^oE 28.1^oS$)/B($85.3^oE 21.6^oN$) separated 943km. In this case the profiles, from the IRI mode, are clearly distinguished, being the discrepancies more noticeable in the case of electron density (left panel). The inversion corresponds to an occultation of the PRN21 at the epoch 1995 October 18th, 5h45minUT.

Table 6.1 gives the average values of $RMS_{profile}$ and difference in NmF2 corresponding to the 209 occultations processed. It can be noted that in all cases the differences are expected to be lower in the case of Shape functions.

	$RMS_{profile}$	Peak
Electron density profiles	53%	35%
Shape functions	16%	3%

Table 6.1: Average figures (computed as the overall RMS divided by the mean value) of differences between Electron density profiles and Shape functions at points A and B of 188 occultations of the GPSMET satellite during 1995 October 18th using the IRI model to simulate the electron density. The maximum distance between A and B points has been limited to 2000km.

In both cases, the difference between profiles will be greatly affected by the distance between the A and B points. Figure 6.4 plots the evolution of the difference against the distance between the A and B points. It is interesting to point out that, as expected, with electron density profiles the differences between the profiles at A and B increases faster with distance compared with the shape functions.

As a final conclusion of this study, the histogram depicted in Figure 6.5 shows that the differences among shape functions within the location marked by the footprint of an occultation are smaller than the case of spherical symmetry.

Even the fact that the use of real data is not as well behaved as the case of the IRI, it can be stated that the use of separability hypothesis overcomes the classical assumption of spherical symmetry, thus providing a more realistic approach to the inversion of profiles with Abel inversion.

6.2 Upper Ionosphere and Plasmasphere estimation

The other issue that has to be taken into account when processing occultations is the contribution of the electron density above the LEO orbit which has to be modeled somehow to correctly invert the GPS observations of STEC. This can be done by making an exponential extrapolation of the profile as done in [Hernandez-Pajares et al., 2000] or in the data as in [Hajj and Romans, 1998]. According to [Schreiner et al., 1999] this approach of exponential extrapolation is more appropriate than the use of a climato-

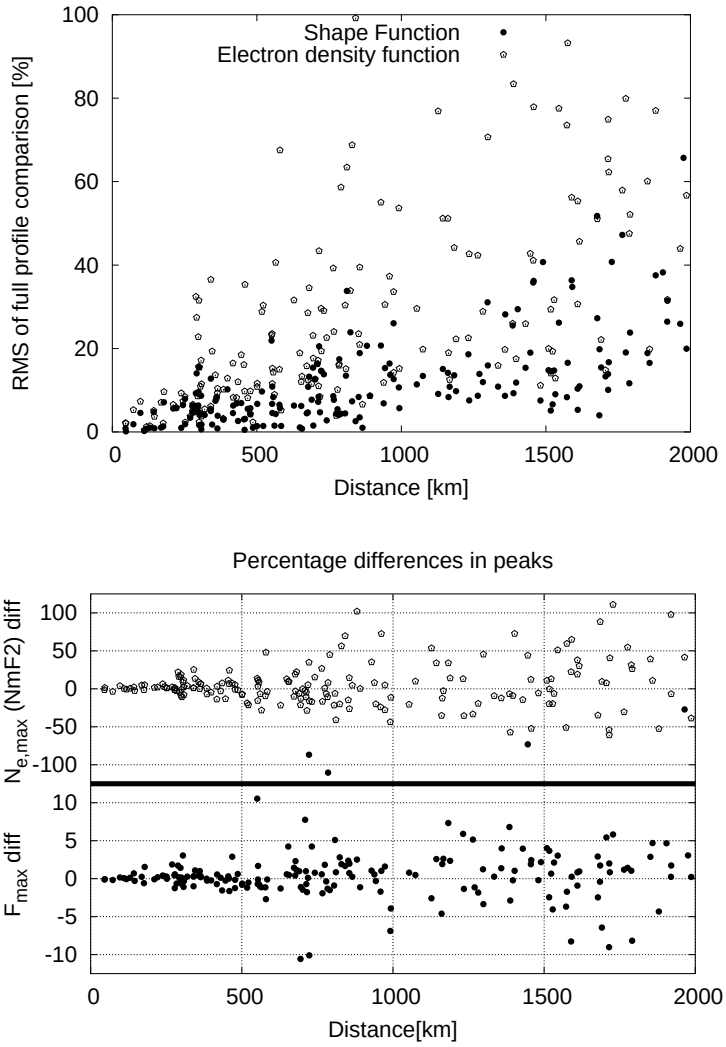

Figure 6.4: (Upper Panel) Evolution of percentage difference ($RMS_{profile}$) against distance. (Lower panel) Evolution of percentage difference (Difference in peak) against distance. Note that although the plots are similar, the scale is 10 times smaller. These graphics have been obtained simulating with IRI the profiles at the corresponding locations A/B of the occultations with GPSMET that took place during day 1995 October 18th.

logical model since it may not be accurate enough. Although this issue may not be critical for LEOs such as GPSMET or SAC-C (with nominal orbits at 750km and 700km respectively), it is a crucial point to be considered with very low earth orbiters such as CHAMP, which has an initial orbit of 450km, but it will descend to 300km in its life-cycle of 5 years due to the atmospheric

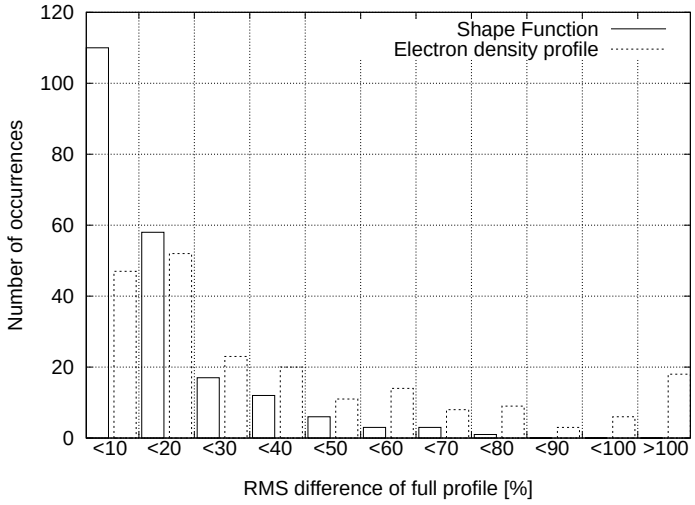

Figure 6.5: Histogram with the number of occurrences for each bin of percentage difference of profile

drag. A possible solution to the upper ionosphere and plasmasphere issue is found in [Jakowski et al., 2002] or [Jakowski et al., 2003], where the inversion is assisted with a "first guess" extracted by a Chapman layer model for the topside ionosphere.

In this work, an alternative way described in [Garcia-Fernandez et al., 2003b] is proposed to tackle this issue. The contribution of the electron density above the LEO orbit is not modeled but estimated. To do this, the positive elevation data gathered by the LEO GPS POD receiver (used to compute the satellite position) is jointly processed with the negative elevation data gathered by the LEO GPS limb sounder receiver (used to obtain the vertical profiles of ionospheric electron content or other vertical profiles of the neutral atmosphere). The key issue to take into account when estimating this contribution is related on how to distinguish between the instrumental bias and the upper ionospheric/plasmaspheric contribution. Since the geometry of the occultation is typically good enough (with large variations in the mapping function, see Section 2.2.1), these two quantities can be estimated in a reasonable way.

6.3 Model

As in the case of ionospheric tomography, the geometric free combination of phases (i.e. $L_I \equiv L_1 - L_2$) has been used as the basic observable. The choice of this observable is due to the fact that the noise level of the phase

observations is lower than the code observations. Nevertheless, the problem to the ambiguity and cycle slips has to be considered. Although a coarse alineation with the P_I is done, the ambiguity has to be dealt with somehow in order to obtain good inversions.

Starting from the discretised approach of the Abel inversion with STEC data explained in Section 4.1.2 and using both expressions 4.17 and 6.2, the L_I can be expressed as:

$$\begin{aligned} L_I(n) &= b_I + \alpha \cdot l_{p,n} \cdot F_p \cdot VTEC(\lambda_{p,n}, \phi_{p,n}) + \\ &+ \alpha \cdot \sum_{k=1}^{n} l_{k,n} \cdot \left[VTEC(\lambda_{k,n}, \phi_{k,n}) + VTEC(\lambda'_{k,n}, \phi'_{k,n}) \right] \cdot F_k \end{aligned} \tag{6.5}$$

where $\alpha = 1.0506 m_{delay} m^2/10^{17} electron$, b_I is the instrumental bias, $VTEC(\lambda, \phi)$ is the VTEC at the geographical coordinates λ and ϕ (for longitude and latitude respectively) and F denotes the Shape function to estimate in the process. Note than the unknown variable to solve F_p is the element of the Shape function that accounts for the contribution of the electron content above the LEO orbit. The schematical view of this expression using the same notation can be seen in Figure 6.6

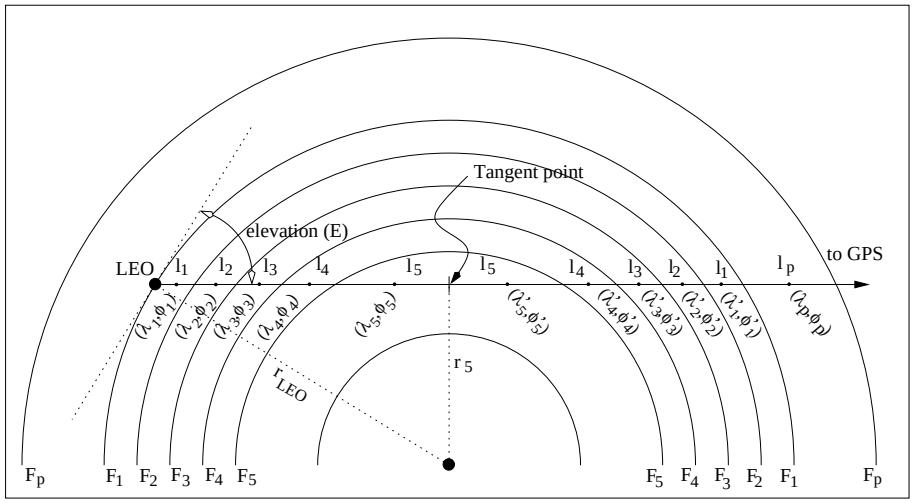

Figure 6.6: Modeling of STEC assuming separability.

Therefore, with the observations of the L_I it is possible to construct a system of equations. This system is solved using the Linear Mean Squares technique, thus solving for the variables corresponding to the bias (b_I) and the Shape function under the LEO orbit (F_k) and above (F_p). Were F_p and b_I not present, this system could be solved recursively.

The geocentric distance for each layer under the GPS LEO orbit are the corresponding geocentric distance of the tangent point, computed as:

$$r(n) = r_{LEO}(n) \cdot cos(E(n)) \tag{6.6}$$

Regarding the height value corresponding to the F_p, since this value is assumed constant in the whole layer, it is set to 1000km (upper limit boundary of the ionosphere considered in this model), but the layer thickness is, in fact, the difference between this upper boundary and the GPS LEO nominal orbit.

6.4 VTEC and spherical symmetry

This section studies particular simple cases of VTEC distributions that lead to a fulfillment (partial or total) of the spherical symmetry assumption. Two cases are considered, when VTEC values are constant and when VTEC is linear.

Constant VTEC

In the first case, that is when VTEC is constant (let us say equal to 1), the solution is equivalent to the spherical symmetry approach, so F becomes N_e (see Equations 4.17 and 6.5).

Linear VTEC

A slightly general case occurs when the VTEC has constant gradients (i.e. linear behavior of VTEC). In this case, only the VTEC values at the different tangent points coordinates are necessary to invert the occultation. This result can be obtained taking into account the symmetry of the occultation geometry (i.e. for a given ray, the distance from the tangent point to both centers of a given layer is the same, see Figure 6.6). Therefore, the sum of both VTEC's corresponding to the same layer but to different geographical locations (see Figure 6.7, where the geographical coordinates of the ray are projected onto the VTEC plane) becomes:

$$\begin{aligned} &VTEC(\lambda, \phi) + VTEC(\lambda', \phi') = \\ &= VTEC(\lambda_T - \lambda_F, \phi_T - \phi_F) + VTEC(\lambda_T + \lambda_F, \phi_T + \phi_F) \end{aligned} \tag{6.7}$$

If the VTEC is driven by a linear function of the longitude and latitude, it is easy to demonstrate that $VTEC(\lambda, \phi) + VTEC(\lambda', \phi') = 2 \cdot VTEC(\lambda_T, \phi_T)$.

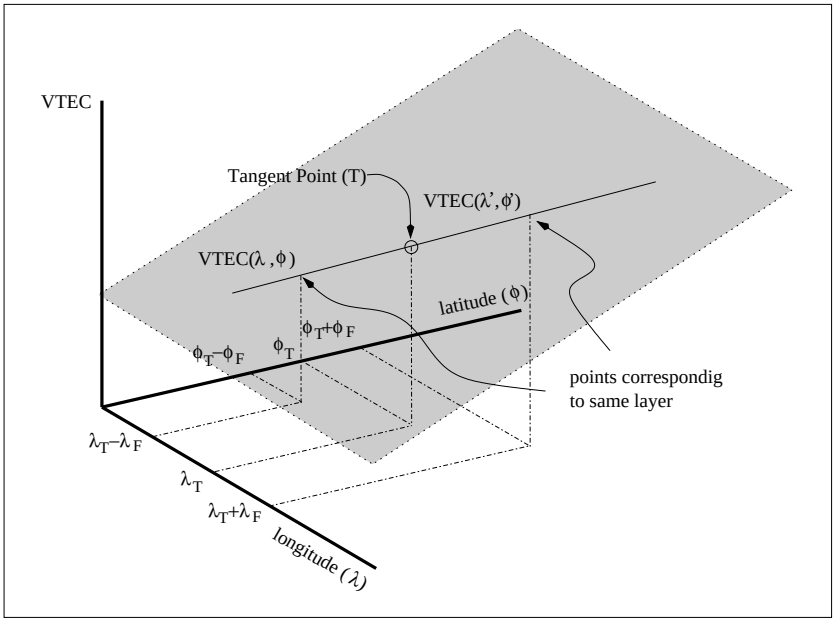

Figure 6.7: Constant gradients of VTEC simplify the Separability hypothesis inversion

That is, when the VTEC follows a linear dependence (i.e. it is defined by a plane), the spherical symmetry is verified for a given ray and only the value of the VTEC at the tangent point location is needed to invert that ray. Nevertheless since the tangent point varies with the ray, different VTEC values for the different rays are needed.

To sum up, the proposed approach verifies that:

1. With VTEC constant it yields to an equivalent solution to spherical symmetry.
2. With VTEC linear, the spherical symmetry assumption applies only within a ray, but different values of VTEC are needed for each ray in order to invert the STEC and obtain the electron density profile.
3. With VTEC non-linear, spherical symmetry is not applicable.

6.5 Results with GPSMET data

6.5.1 Synthetic data (IRI)

The comparison with synthetic data is performed since it offers a valuable possibility to perform the proof of concept and the comparison of the inverted

electron density profiles with true values of electron density. Moreover, there is no **co-location** error, therefore it is possible to obtain the electron density at the exact desired longitude, latitude and time. Two consequences of this fact are derived:

- When providing the VTEC values to the model, no interpolation to obtain these values is needed, thus avoiding the corresponding interpolation error.
- There is no spatial/temporal mismatch (i.e. co-location) error with respect to the truth to compare.

Therefore, since the most important sources of errors are not present in this environment, this study will give an overview of how good is the model itself (the best performance one can expect from it). Nevertheless, since this is a simulated environment, a deeper study with real data is necessary in order to assess the performance of the method in real circumstances. Obviously, in the real cases the errors are expected to be larger.

The study presented in this section consists basically in inverting the "simulated" observations. That is, considering the actual geometry and epoch of the occultations (i.e real line-of-sights), the IRI model is run and the STEC corresponding to each ray of the occultation is simulated. Once all rays are simulated, the inversion is performed and the profile of electron density is obtained. The peak of electron density (i.e. NmF2) and its height (i.e. hmF2) are extracted and compared with the values provided by the IRI model at the exact time and coordinates of the occultation occurrence.

The data has been simulated for the GPSMET observations on 1995 October 18th (approximately 200 occultations were processed).

Table 6.2 summarizes the results considering spherical symmetry and separability hypothesis. It can be seen that separability assumption improves in all circumstances those obtained with spherical symmetry (an average improvement of 25% to 30%). Note that, on the other hand, this improvement does not affect to the hmF2 estimation, compared with spherical symmetry.

6.5.2 Real data

Scenario

In order to confirm the improvement against the spherical symmetry approach, a data set using real data has been considered. This results are extracted from [Garcia-Fernandez et al., 2003a] and are an extension of the study presented in [Hernandez-Pajares et al., 2000]. The data set consists in

		NmF2 comparison			hmF2 comparison	
	# comp	bias $[10^{10}\ e/m^3]$	σ $[10^{10}\ e/m^3]$	RMS [%]	bias [km]	σ [km]
Night	81	**-0.1**	**1.6**	**10.1**	**-4.6**	**11.0**
		0.3	*2.7*	*16.8*	*-7.1*	*10.3*
Dawn	58	**-0.6**	**1.2**	**4.6**	**-2.5**	**10.9**
		1.3	*2.7*	*10.5*	*-2.9*	*11.6*
Day	68	**0.5**	**4.4**	**8.0**	**-6.9**	**12.9**
		0.5	*7.0*	*12.6*	*-6.8*	*12.3*

Table 6.2: Table for NmF2 and hmF2 comparison for GPSMET satellite using the IRI model, 1995 October 18th. In bold are the values corresponding to **Separability assumption** and italics mark the values of *Spherical symmetry* assumption. Although the absolute errors for the different periods are similar, the variation of the electron density values with the day period influences the relative errors.

a 11 day period, from October 10th 1995 (day of year 283) to October 21th 1995 (day of year 294). LEO data from the GPSMET satellite were processed with the aid of the VTEC maps computed and provided at UPC in IONEX format for this period. These maps provided to the improved Abel inversion method with information of the horizontal variation of the electron density.

To evaluate the Abel estimations of electron densities and heights, the occultations have been checked with the measured parameters given by ionosondes. These were mainly located in Europe, North America and Australia. Moreover, there are few comparisons for low latitudes due to the observations of the Taiwan ionosonde. This period also includes not only quiet ionospheric conditions but an ionospheric disturbance over central Europe during the day 1995, October 19th (day of year 292). The Dst indicates the presence of a disturbance beginning at 1995 October 18th 21hUT approximately (upper plot of Figure 5.6).

Estimation of electron content above LEO orbit

In order to check the upper ionosphere and plasmaspheric estimation, a voxel model, see Section 3.2.1, has been used joining the available positive elevation data (with an elevation mask of 10^o), using similar procedures to obtain VTEC estimates from ground GPS data ([Hernandez-Pajares et al., 1999]). Previous works have already shown that these methods can provide with very accurate determinations of VTEC ([Hernandez-Pajares et al., 1998]).

On the other hand, the estimation with the proposed method has been obtained processing each occultation independently using both positive and negative elevation data. Figure 6.8 depicts the comparison between these two approaches. The values corresponding to the same geomagnetic latitude have been averaged in longitude. It can be seen how the estimation shows the expected increase of few TECU of the upper ionospheric and plasmaspheric TEC in low geomagnetic latitude. A similar result is obtained during the night (lower panel of Figure 6.8), where the expected decrease is stated during this period.

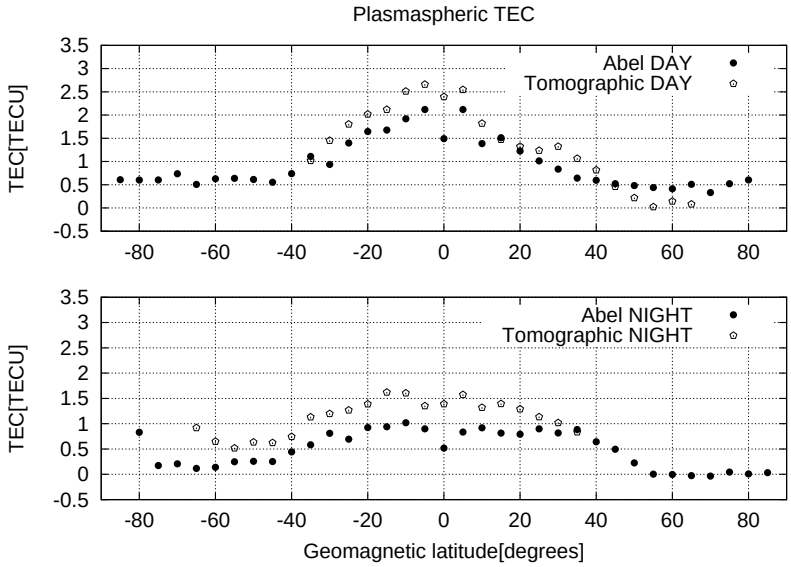

Figure 6.8: Comparison of Plasmaspheric TEC estimated by F_p and the estimation with voxel model.

Note that in the case of a bad estimation of the upper ionosphere and plasmaspheric estimation, the rest of the profile will be affected, due to the recursivity of the method. Therefore, in fact, the same profiles are a type of test on the validity of the upper ionospheric estimation.

Comparison with ionosonde

As a general procedure for comparison with ionosondes, it has been considered that for a single occultation and ionosonde, the valid comparisons were those made with the ionosonde measurements comprised in an interval of 1 hour centered at the epoch that the occultation took place. Besides, the maximum distance between an ionosonde and the occultation

(i.e. co-location distance) was set at 2000km. Previous works (see for instance [Hajj and Romans, 1998] or [Schreiner et al., 1999]) consider shorter co-location distances of 1500km approximately.

It has to be taken into account that the separability hypothesis implies the proportional relationship between the NmF2 and TEC and, consequently, a constant slab thickness during the occultation (Expression 6.1). Therefore it is expected that a deviation from this assumption may cause a mismodelling. This can happen specially during dawn and dusk periods (as it can be seen in Figure 6.9) or with ionospheric irregularities (i.e. when the slab thickness does not show a constant behavior).

Therefore, the dependency of the slab thickness in function of the local time has been studied for the period considered (see Figure 6.9) in order to check the consistency between the measured values of peak density from the ionosondes and VTEC computed from the ground GPS data. In this figure it can be seen the presence of unrealistic values of τ. These values can be due to ionosonde measurement, specially during night periods, or VTEC interpolation. The slab thickness values under 175km or above 1000km have been discarded since this may be due to a large error in the ionosonde NmF2 value and/or VTEC interpolation causing a bad comparison.

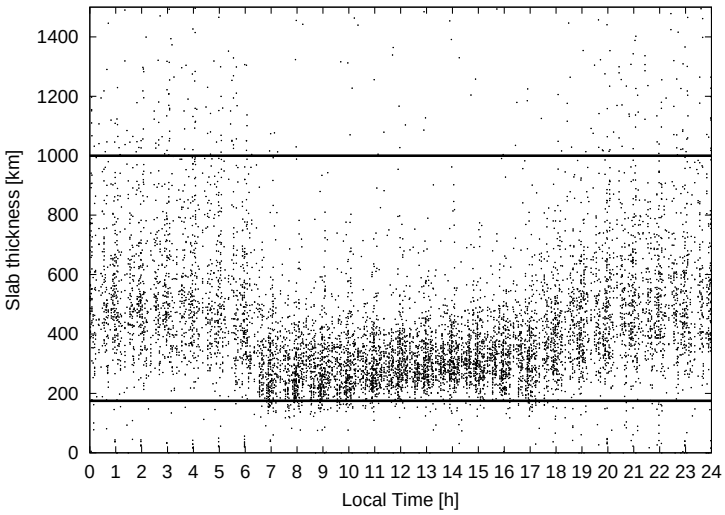

Figure 6.9: Dispersion plot of slab thickness in function of local time for the period from 1995 October 10th to 1995 October 21st. The values of NmF2 were obtained from the 52 ionosondes available during this period. The boundaries to discard unlikely values of the slab thickness have been set at 175km and 1000km (also shown in the plot).

From expressions 6.2 and 6.1, it can be seen that the inverted occultation

can give a measure of the slab thickness by inverting the shape function at the peak of the profile ($\tau_{occultation} = 1/F(hmF2)$). Therefore, the same criteria of slab thickness applied to ionosonde/TEC measurements explained above has been applied to each occultation as well. This filter rejects around 10% of comparisons due to unrealistic ionosonde/TEC measurements and/or bad inverted occultation. These outliers are caused mainly by ionosonde data (approximately 70% of the rejected comparisons, the remaining 30% were due to occultation data). For both the ionosonde and occultation data, the measurements with slab thickness above 1000km were located during nighttime, coinciding with very low electron density values. On the other hand, daytime contained the majority of rejected comparisons caused by a slab thickness under 175km.

Frequency estimations

Usually, the Abel inversion literature provides with the comparisons between ionosonde and Abel inverted profiles in frequency units rather than electron density ones. In order to place this work in context with similar works, units are chosen to be frequencies as well. Following this criteria, the Abel profile values of the maximum electron density at the F2 and E layers (NmF2 and NmE respectively) have been transformed to the corresponding critical frequencies (foF2 and foE respectively) using Expression 1.24. Note that the quadratic relationship implies that an error in frequency of 10% corresponds to an error of 20% in density approximately (a factor of 2), that is, errors on frequency estimation will be approximately the half value of the N_e estimation.

Regarding the estimation of the F2 layer critical frequency (i.e. foF2), table 6.3 summarizes the comparison of the performance between the spherical symmetry approach of Abel inversion and the one assuming separability. It is expected that during the periods in which the hypothesis of proportionality of the VTEC and density is clearly unrealistic (i.e. slab thickness not constant), the results worsen. The table shows how in the cases mentioned in Section 6.1 (low latitudes, high geomagnetic activity, dusk and dawn) the performance with respect to the ionosonde measurements are worse.

Even during occurrence of the above mentioned factors, the introduction of VTEC information in the Abel inversion improves the estimations obtained assuming spherical symmetry. In fact, the average improvement is about 30%.

Figure 6.10 shows a graphical interpretation of the discrepancies for two particular examples of comparison between ionosonde and inversion. The effect of the slab thickness in the comparisons is shown. Upper plot cor-

		N.comp	Sep.Hyp. RMS: MHz [%]	Sph.Symm RMS: MHz [%]
Quiet ionosphere				
Low	Day	177	1.2 [16.2]	1.6 [21.4]
latitudes	D&D	10	0.5 [9.7]	0.8 [14.5]
$0^o \pm 30^o$	Night	100	1.1 [27.6]	1.3 [31.7]
Mid&high	Day	2054	0.7 [11.6]	1.1 [17.8]
latitudes	D&D	908	0.8 [19.1]	1.1 [25.9]
$\pm 30^o \pm 90^o$	Night	1122	0.6 [17.6]	0.8 [23.9]
Disturbed ionosphere				
Europe	Day	105	0.9 [17.7]	1.6 [31.2]
	D&D	94	0.7 [18.2]	1.2 [30.8]
	Night	32	0.4 [16.1]	0.8 [34.9]

Table 6.3: Table of foF2 errors with respect to Ionosonde measurement. The error is Absolute RMS in MHz and Percentual relative RMS difference in brackets. The number of comparisons is also given.

responds to a shape function of an occultation taking place near College (Alaska, W147.8 N64.9). In this case, the slab thickness behaves almost constantly, therefore the comparison is better than in the case in which the slab thickness is not constant. This is the case of the lower plot, where the electron density peak increases while the VTEC at the ionosonde location (Taiwan, E121.2 N25.0) decreases. This behavior is not reflected in models such IRI, in which in harsh conditions such as maximum in the solar cycle and low latitudes, the VTEC always behaves in the same way as the electron density.

The increase of distance between the ionosonde and the occultation (i.e. lack of co-location) is an additional source of error. Figure 6.11 shows how the error increases as the co-location decreases (distance increases). Nevertheless, since an appropriate VTEC is considered to obtain the $N_e(\lambda, \phi, h)$ profile from a shape function, the error contribution of co-location is diminished when the assumption of separability is considered. In the case of the spherical symmetry, the error in the foF2 estimation increases by an average value of 0.40MHz each time the co-location distance is increased by 1000km. In the case of the separability assumption, this rate is reduced to 0.14MHz/1000km, showing more robustness of this approach with regard to the co-location error. This plot shows an average bias of -0.1MHz in the estimation of the foF2 using the separability approach. The bias shows a certain local time dependency (i.e. with the GPSMET orbit) in both the spherical symmetry

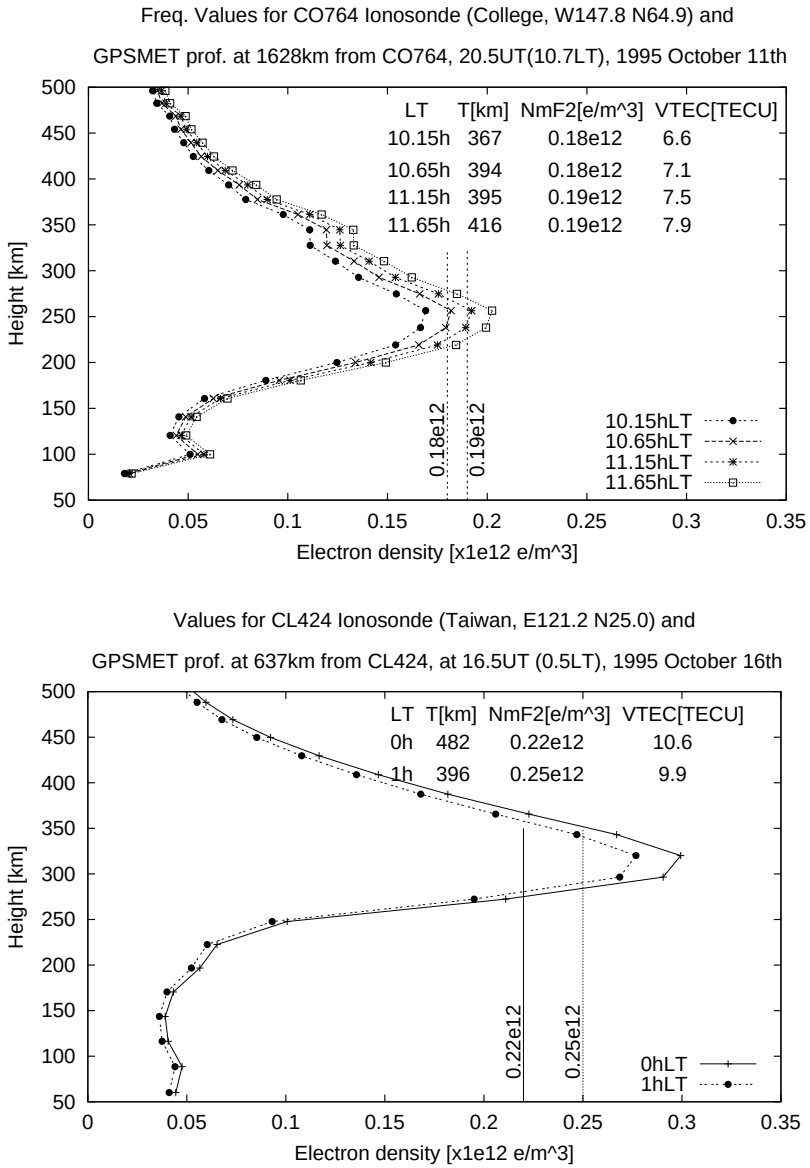

Figure 6.10: Effect of the variation of the slab thickness in the comparisons. The plots correspond to 2 different shape functions. The NmF2, VTEC and slab thickness (T) at the ionosonde location are indicated at the given epochs. To obtain the electron density profiles the shape function has been multiplied by the given VTECs.

and separability hypothesis approach, this reported negative bias corresponds to the daytime period, which contains the larger number of comparisons

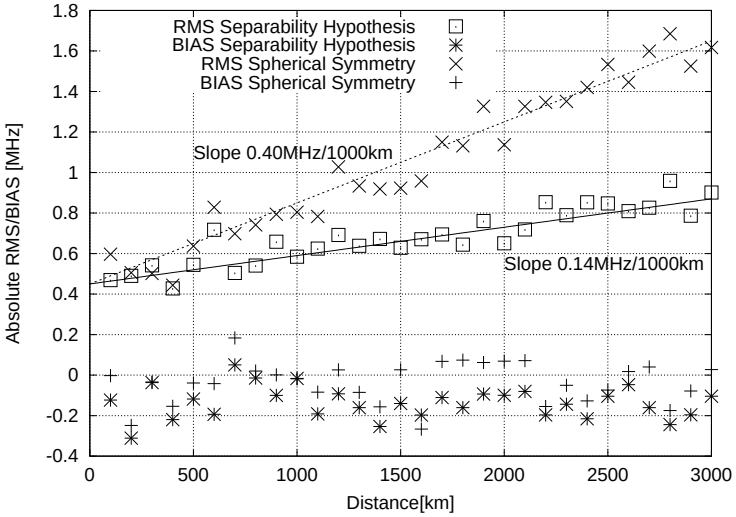

Figure 6.11: Effect of the co-location distance to the absolute RMS error of foF2 estimation with respect to Ionosonde measurements. Processed period of GPSMET data from 1995 October 10th to October 21st. A total number of 52 ionosondes were used for comparison (mainly located at Europe and USA).

(nearly 30% of all comparisons correspond to the time period from 9hLT to 11hLT, when the GPSMET travels from North to South, see Figure 6.12). The bias is due to a mismodelling caused by the assumption of a shape function as a profile descriptor. This bias can be seen as well in the integral of the shape function, which should be 1 ideally. Nevertheless, actual inversions offer discrepancy with respect to this value. The typical values of this integral for the occultations processed is around 0.8, which explains this negative bias.

Regarding the estimation of the E and E-sporadic layers (foE and foEs), the comparative performance of the two Abel approaches has been studied as well. As mentioned in previous sections, since the Abel inversion is a recursive method in which the upper layers are solved before the lower-most ones, the error in the estimation of the former can affect dramatically the latter. Although the importance of this effect may depend on the occultation, the assumption of separability helps to diminish this effect (see Figure 6.13 and Table 6.4). To compare the two approaches for the Abel inversion, the occultations with the presence of a peak in the interval 90-130km have been searched for. The number of comparisons are less than the case of the foF2 for several reasons: the most important is that the E layer is not always detected with the sampling rate provided by the GPSMET, other reasons are due to the fact that the E-layer is mainly detected only during daytime.

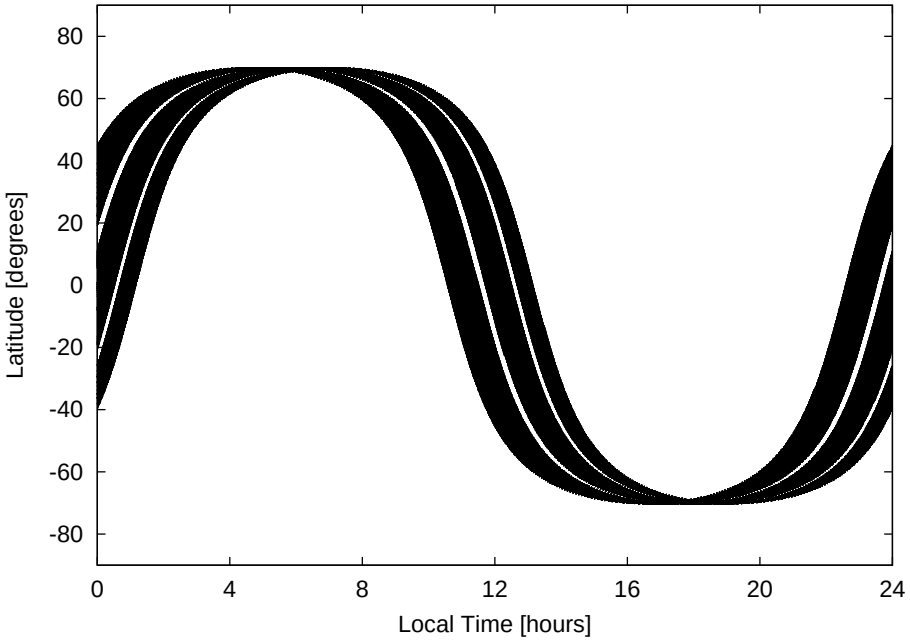

Figure 6.12: GPSMET orbit in function of local time for the period 1995 October 10th to October 21st. Note that the pass from North to South take place during noon period.

Again, the values of the shape function are multiplied by the corresponding VTEC at the location of the ionosonde. Afterwards, it has been compared with the values of foE and foEs provided by the ionosonde. The discrepancies are summarized in Table 6.4.

	N.comp	Sep. Hyp. RMS: MHz [%]	Sph. Symm. RMS: MHz [%]
E layer	135	0.4 [17.1]	0.7 [28.5]
Es layer	35	0.5 [16.2]	1.0 [30.4]

Table 6.4: Table of foE errors with respect to Ionosonde value. The error is Absolute RMS in MHz and Percentual relative RMS difference in brackets.

As in the case of foF2, the results considering separability hypothesis improve by an average figure of 40% those obtained with spherical symmetry.

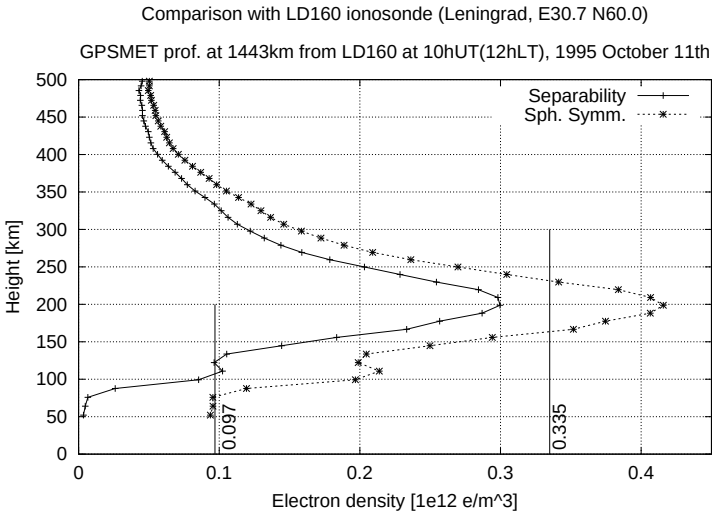

Figure 6.13: Effect of accumulative errors on the computation of the E layer electron density. The errors in the estimation of the upper layers strongly affects the lower-most layers. This particular example corresponds to an occultation of the GPSMET with the PRN20 at 1995 October 11th (day of year 284), 10hUT(12hLT), at E43.3 N44.9, compared with the corresponding NmF2 and NmE values obtained with the Leningrad Ionosonde.

Height estimations

The performance of Abel transform with regard to the estimation of true-height profiles of electron densities, and in particular the estimation of the electron density peak height value (i.e. hmF2), is an issue that the same attention has not been paid in previous works as in the case of electron density. If synthetic data are used, the comparison between vertical and inverted profiles is direct. The hmF2 estimation using this type of data are in agreement with the true values at the level of 5-10km (see for instance [Hajj et al., 2000] and Section 6.5.1).

Nevertheless, the comparison with real data is not so easy due to the fact that the number of direct measurements (i.e. data from Incoherent Scatter Radar) are lower and sparse, therefore it is necessary to obtain the hmF2 using other methods for a wider comparison (see Section 1.4.1). The Dudeney formula (Expression 1.27) has been used in [Jakowski et al., 2002] for the purpose of comparison with the hmF2 value obtained with the inversion of CHAMP occultations, reporting an RMS of the discrepancies of about 45km. An additional method to the Dudeney formula is the POLAN true-height inversion, that provides real-height profiles of electron density up the

hmF2 height. In Figure 6.14, particular examples of the performance in the profiles computed with Abel inversion compared with a standard method of inverting ionograms such as POLAN are shown.

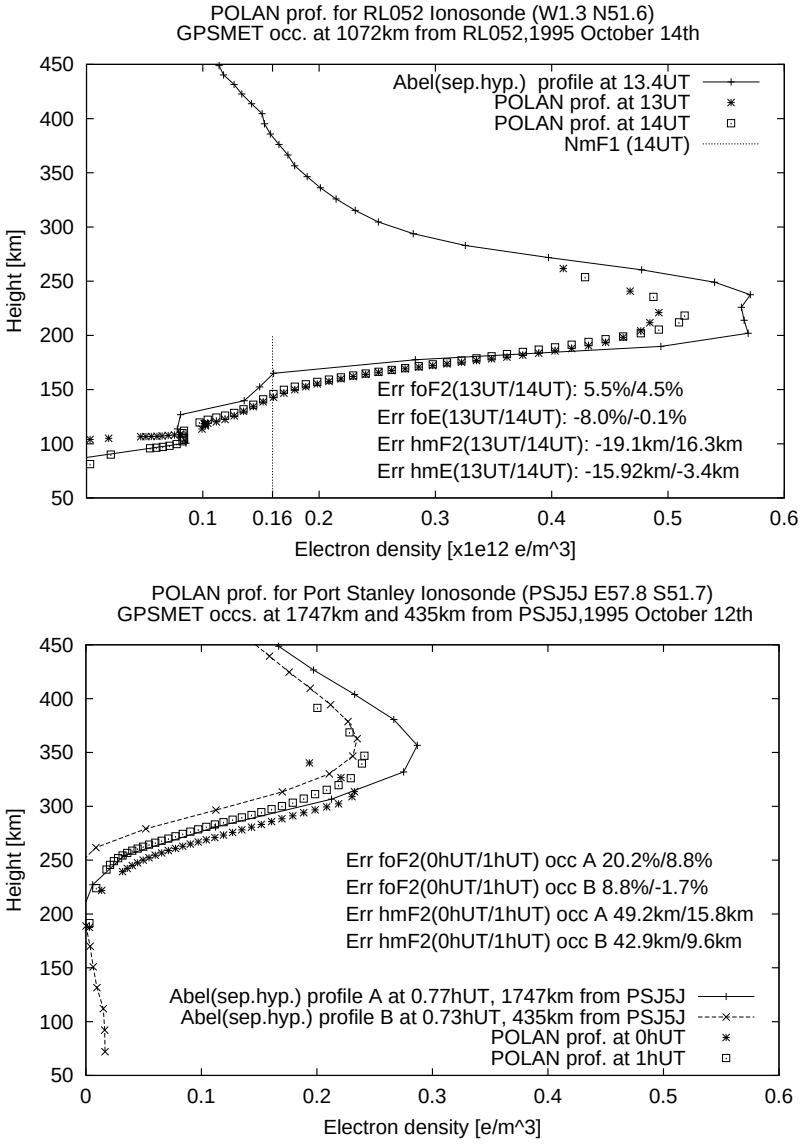

Figure 6.14: Inverted profiles using GPSMET data and separability hypothesis. The comparison is made with POLAN profiles obtained from ionogram data.

In [McNamara et al., 1987], it was reported a bias of the Dudeney formula with respect to the POLAN method. Moreover it was stated that this bias

was related to the ratio between the peak frequencies of the F2 and E layers ($foF2/foE$). Despite the fact that the comparative study of the hmF2 values obtained by both methods is beyond the scope of this Doctorate thesis, table 6.5 contains a comparison between these methods and additionally the hmF2 values extracted from the profiles inverted with Abel transform for the ionosondes of Lerwick, Chilton and Port Stanley. The POLAN profiles have been obtained from [World Data Center-A, 2003] and the expected error for the estimation of the hmF2 using POLAN reported for this dataset is 3km approximately. In the case of the Dudeney formula, [McNamara et al., 1987] applied the condition $foF2/foE > 1.215$ to obtain reliable measurements of hmF2. For coherence with the results of that work, the same condition has been applied, although other authors are more strict with this conditions (see for instance [Rishbeth et al., 2000]).

	$foF2/foE \leq 2$			$foF2/foE > 2$		
	N.comp	bias [km]	σ [km]	N.comp	bias [km]	σ [km]
POLAN-DUD	39	15.9	20.8	174	0.5	9.3
Abel-POLAN	65	-12.6	27.0	252	-0.8	22.1
Abel-DUD	65	4.1	21.1	252	0.8	23.1

Table 6.5: Inter-comparison between the POLAN, Dudeney formula and Abel inversion for hmF2 estimation for the ionosondes of Lerwick, Port Stanley and Chilton. Only the common data between methods have been considered. The values for the bias and standard deviation are expressed in km.

Following [McNamara et al., 1987], the height comparisons obtained in this work have been divided according to the ratio $foF2/foE$. It can be seen that the bias follow the same behavior (the larger the frequency ratio the lower the bias). Regarding the standard deviation in the comparison of Abel with the other models, it is similar in both cases, close to 25km.

A summary of the Abel inversion performance as an hmF2 estimator (compared with the Dudeney formula, using all available ionosonde data) is showed in Table 6.6. These results indicate that the dependency of the bias with the ratio $foF2/foE$ has a special significance in the RMS comparison.

Figure 6.15 shows the bias and standard deviation for several ionosondes. It can be seen that the bias depends on the ionosonde, which in turn causes the overall RMS to suffer a certain increase. Note in the figure a slight increase of the bias as latitude decreases, this could be explained by the fact that the assumption of the separability for the lower latitudes is valid to a

Abel-DUD	N.comp	bias [km]	σ [km]
$foF2/foE \leq 2$	682	- 2.7	24.0
$foF2/foE > 2$	1775	-10.8	25.8

Table 6.6: Comparison with Dudeney formula for all available ionosondes. The values for the bias and standard deviation are expressed in km.

certain extent (i.e. for these latitudes, only one shape function can not fully describe the height variation of the profile).

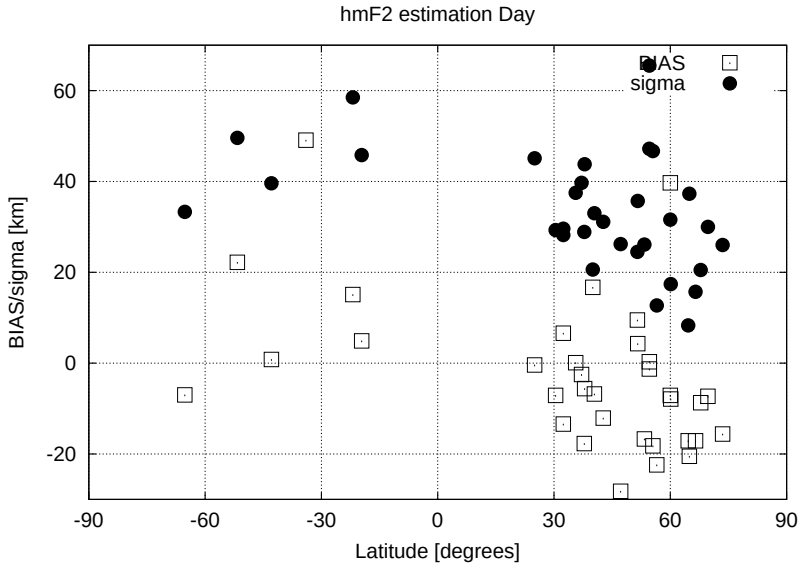

Figure 6.15: Latitude variation of the standard deviation. The bias and standard deviation are plotted for each ionosonde. The reference values for the hmF2, due to its wider availability, have been obtained from the Dudeney formula applied to the period of 1995, October 10th to 1995, October 21st. There were 32 ionosondes for which the parameters foF2, foE and M3000F2 were simultaneously available.

The GPSMET data used in this work were sampled at every 10 seconds. This implies that the height resolution is of few kilometers in the upper layers and it decreases for the lower layers reaching to the impact parameter separation of 20km near the peak of the F2 layer and below. Therefore, the error due to the discretisation is about 10km. Regarding the discrepancies with the reference values of hmF2 using separability hypothesis and spherical symmetry, these are small enough to state that those methods offer the same performance with regard to height estimation.

6.6 Results with concurrent missions: SAC-C and CHAMP

Using the same technique applied to GPSMET radio occultations and the comparison method with ionosonde data, a test with the SAC-C and CHAMP radio occultations has been carried out as well. An important point of missions taking place at the same time is a better coverage on the ionospheric sounding. Moreover, with concurrent missions it is possible to perform an intercomparison between both satellite and to test the proposed algorithm in two different datasets for the same time period.

An additional difference with respect to the GPSMET dataset used in the previous study is that the sampling rate of the data from SAC-C and CHAMP satellites is 0.1Hz for the POD receiver and 1Hz for the data related to radio occultations. This higher sampling rate is translated in vertical profiles with higher resolution, thus allowing the imaging of features or characteristics of the profile that could be hidden otherwise.

The difference of CHAMP satellite with respect to SAC-C and GPSMET is its low orbit. This offers a challenge regarding the upper ionosphere and plasmasphere content modeling. For LEOs at high altitudes, the electron content above its orbit can be approximated using an exponential extrapolation (applied to the data as done in [Hajj and Romans, 1998] or in the profiles as in [Hernandez-Pajares et al., 2000]). Nevertheless, when the orbit is low as the CHAMP, the electron content above has to be modeled more accurately. A possible approach can rely in the use of an external model to account for this electronic content as done in [Jakowski et al., 2002].

In the case of the proposed method, the electron content is estimated through the variable F_p (see Section 6.3). The comparisons given in this section provide an assessment on how this electron content affects the statistics of frequency and height.

A slight modification with respect to the GPSMET data has been applied for these satellites. The reason for this change of implementation is that for the SAC-C and CHAMP satellites, two different receivers are gathering the GPS data:

1. The Precise Orbit Determination (POD) receiver, used to obtain the LEO position. It gathers data with positive elevation.

2. The Limb Sounder receiver, used to invert the radio occultations. It gathers data with negative elevation.

Therefore, two receivers imply two different phase ambiguities and therefore two different biases. According to this issue, the modified algorithm

estimates two different biases (one for each receiver). Strictly speaking, it would be necessary to add an additional bias to estimate for each ambiguity of the phase (this was valid for the GPSMET as well). Nevertheless, specially in the case of negative elevation data, the amount of data is not enough to solve for both the biases and the whole vertical profile. An initial alignment with the code (which does not show the problem of phase ambiguity) diminishes the effect of cycle slips, nevertheless a certain amount of noise due to this alignment is added to the phase.

6.6.1 Scenario

The chosen scenario for the SAC-C and CHAMP GPS data runs from November 1st 2002 (day of year 305) to November 16th 2002 (day of year 320). According to the plot depicting the Solar Activity (see Figure 1.3), this period corresponds to a maximum in the Solar Cycle. The Dst parameter corresponding to the period chosen is depicted in Figure 6.16, showing that the period was relatively quiet in terms of ionospheric activity.

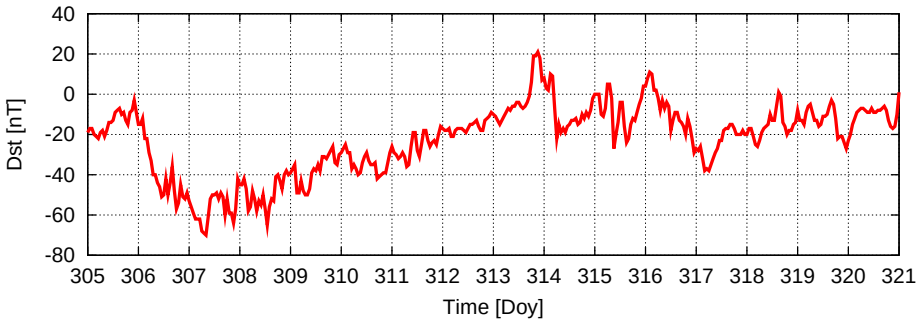

Figure 6.16: Dst parameter from November 1st 2002 to November 16th 2002.

Since the method has been already tested with simulated data from IRI in the GPSMET satellite, this section only contains a comparison with real parameters measured by ionosonde.

6.6.2 Comparison with Ionosonde data

As in the case of the GPSMET, the validation of the occultations has been performed with ionosondes and the slab thickness has been used as a filter to discard doubtful comparisons as well. Although the number of ionosondes (28) is less than in the GPSMET scenario, their sampling rate is 4 times greater in average (ionospheric measurements provided each 15 minutes). In this case, a time filter of slab thickness based on hourly values of bias

and σ has been used to discard outliers (values larger than 3σ have been considered as outliers). Moreover, sudden peaks in the temporal series of the slab thickness have been discarded as well.

For coherence with the previous section, it has been chosen the same co-location distance between the occultation and the ionosonde (2000km) and the same time span centered at the occultation occurrence (1hour).

Frequency comparison

Frequency comparison with the F2 layer peak is done in the same way as in the case of GPSMET. Table 6.7 summarizes this comparison. In all cases the separability approach improves the result of the spherical symmetry by an average value of 57% and 36% for the CHAMP and SAC-C respectively. In Figure 6.17 it is shown the evolution of the RMS of foF2 comparison against distance. Note how, as happened with the GPSMET, the larger the distance between occultation and ionosonde the larger the error of foF2 estimation.

LEO		# comp.	Separability bias [MHz]	σ	Rel. RMS [%]	Spherical Symmetry bias [MHz]	σ	Rel. RMS [%]
CHAMP	Day	2161	-0.7	1.2	13.5	0.0	2.1	21.0
	D & D	101	-0.3	1.0	17.7	-1.7	2.8	53.7
	Night	873	0.0	1.0	18.4	-1.3	2.3	50.0
SAC-C	Day	4934	-0.4	1.2	11.9	0.1	2.0	18.4
	D & D	239	0.1	0.9	16.6	0.0	1.4	26.3
	Night	1289	0.3	0.9	19.1	0.5	1.4	29.0

Table 6.7: F2 layer critical frequency comparison for the SAC-C and CHAMP satellites, using Ionosonde foF2 parameter. Table shows the bias and σ of the comparison (in absolute values of MHz) and the relative RMS (percentual value with respect to the mean value of the ionosonde)

Note the larger differences in the CHAMP satellite between separability and the classical Abel approach. These are due to one of the consequences of assuming spherical symmetry: the bad estimation of the electron content above the LEO, which is caused by the fact that in most cases, assuming a constant value of electron density throughout the cell above the LEO (in the case of CHAMP from 400km to 1000km) leads to a large mismodelling. This results in an additional error that affects the rest of the profile, but specially to the uppermost layers. Since the maximum in the CHAMP satellite is near to its orbit, the comparison with ionosonde can be severely affected. In the case of SAC-C, the satellite orbit is far from the maximum, so this effect is

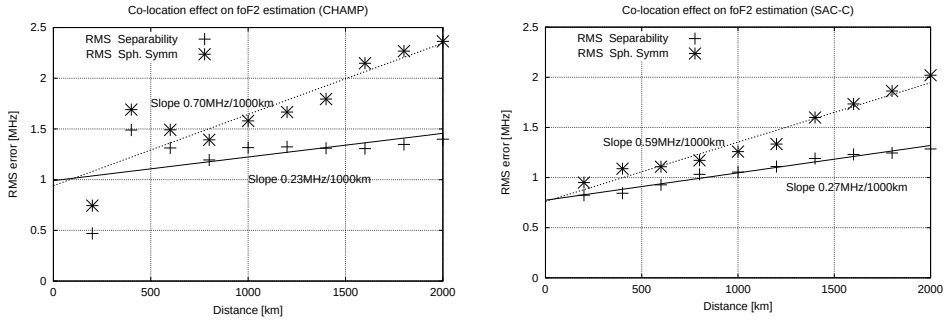

Figure 6.17: Evolution of the RMS (of foF2 comparison) against distance for CHAMP and SAC-C satellites. It is given as well the slope computed as linear regression.

palliated to a certain extent. An example of this phenomena for the CHAMP satellite can be seen in Figure 6.18.

The results regarding the foF2 estimation using spherical symmetry and CHAMP data are analogous than those obtained in [Jakowski et al., 2003]. Although in this thesis work the percentage and absolute values are higher, the co-location distance is larger as well (in front of the radial distance of 8^o, which corresponds to less than 1000km, used in [Jakowski et al., 2003]). Note also that the RMS evolution against distance for the CHAMP satellite increases 0.7MHz each 1000km (in the case of spherical symmetry and for the period studied, see Figure 6.17). If we would consider a geometric distance of 1000km, the absolute error of the foF2 with respect to ionosonde for the method explained in this work and that of [Jakowski et al., 2003] would be similar.

In the case of the E layer, the SAC-C and CHAMP satellites offer the advantage of a higher sampling rate than the GPSMET experiment. This allows to a better detection of small features in height and, in particular, the monitoring of the E-layer. Since ionosonde offers the possibility to monitor the E-layer critical frequency, an additional comparison is also possible. In this context, Table 6.8 summarizes the comparison for both satellites. In this case, since the E-layer is basically detected only during daytime, the comparisons are given for this period only.

Based on the fact that the E-layer is well-behaved, it is possible to establish a simple filter on the E-layer obtained with the inversions, based on the upper and lower limits of the E-layer frequencies measured by the ionosondes. The E-layer values under $1 \times 10^{-7} m^{-1}$ or above $5 \times 10^{-7} m^{-1}$ (shape function units) for the separability approach have been discarded. In the case of the

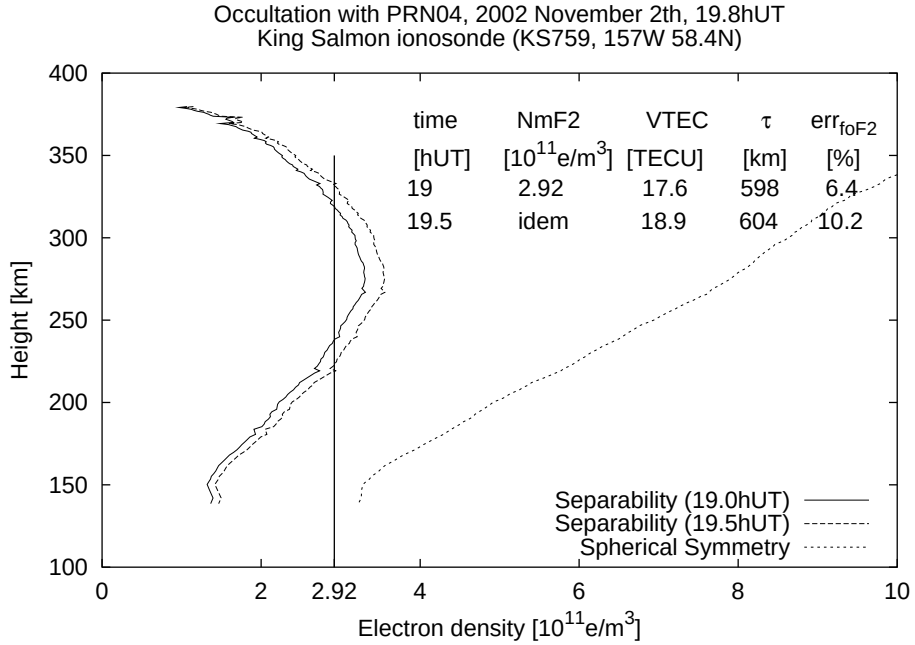

Figure 6.18: Assumption of spherical symmetry affects topside estimation. In this case an occultation with PRN04 at 2002 November 2th (19.8hUT approx) with spherical symmetry and separability are depicted. Values of maximum of electron density, VTEC, slab thickness (τ) and the error in the frequency comparison in the separability assumption case are also given. The profile with separability hypothesis in this case is not realistic, therefore no comparison is given.

LEO	Separability				Spherical Symmetry			
	# comp.	bias [MHz]	σ	Rel. RMS [%]	# comp.	bias [MHz]	σ	Rel. RMS [%]
CHAMP	326	-0.2	0.6	20.7	349	0.0	1.0	33.4
SAC-C	558	0.1	0.7	23.1	567	0.4	1.0	40.4

Table 6.8: E layer critical frequency comparison for the SAC-C and CHAMP satellites, using Ionosonde foE parameter. Table shows the bias and σ of the comparison (in absolute values of MHz) and the relative RMS (percentual value with respect to the mean value of the ionosonde)

spherical symmetry case, these boundaries have been set to $0.2 \times 10^{11} e/m^3$ and $2.5 \times 10^{11} e/m^3$. Note that the differences between assuming spherical symmetry and separability hypothesis are consistent with the GPSMET case (average improvement close to 40%).

Height comparison with Dudeney

As done in [Rishbeth et al., 2000], to estimate the values of hmF2 from ionosonde data using the Dudeney formula, two conditions have been used: $foF2/foE > 1.7$ and $M3000F2 > 2.5$. This filter differs from the one applied in the case of GPSMET ($foF2/foE > 1.215$), which was used for coherence with the POLAN comparison (in this case no comparison with true-height technique is given).

The conditions lead to the fact that the measurements of hmF2 basically correspond to daytime since the restriction on the $foF2/foE$ ratio eliminates the doubtful values, which are mainly during periods outside daytime. A summary of the performance of the Abel inversion regarding the hmF2 value with respect to the ionosonde estimation using Dudeney formula is showed in Table 6.9. From the results of this table, no significative differences between the spherical symmetry and separability approach can be detected. This is justified since the separability leads to a scaling of the shape function by the VTEC resulting in different electron density profiles, but the profile in height remains almost unchanged.

Although being in a maximum of the solar cycle, differences in the hmF2 estimation are similar to those obtained with the GPSMET. These discrepancies of the hmF2 estimation remain below 30km, being similar than the generally accepted error of the Dudeney formula applied to ionosonde data (20km to 30km approximately).

LEO		Separability		Spherical Symmetry	
	# comp	bias [km]	σ [km]	bias [km]	σ [km]
CHAMP	1510	0.5	28.2	1.6	30.7
SAC-C	3010	-3.2	25.8	-3.6	25.9

Table 6.9: F2 layer critical peak height comparison for the SAC-C and CHAMP satellites, using Dudeney formula. The period runs from 2002 November 1st to 2002 November 16th. Results consist in the bias and σ (expressed in units of km) for both approaches of spherical symmetry and separability hypothesis.

In Figure 6.19 it is shown the bias and σ in function of latitude. In this case, the dependency of the hmF2 error with respect to latitude is not as clear as in the case of the GPSMET.

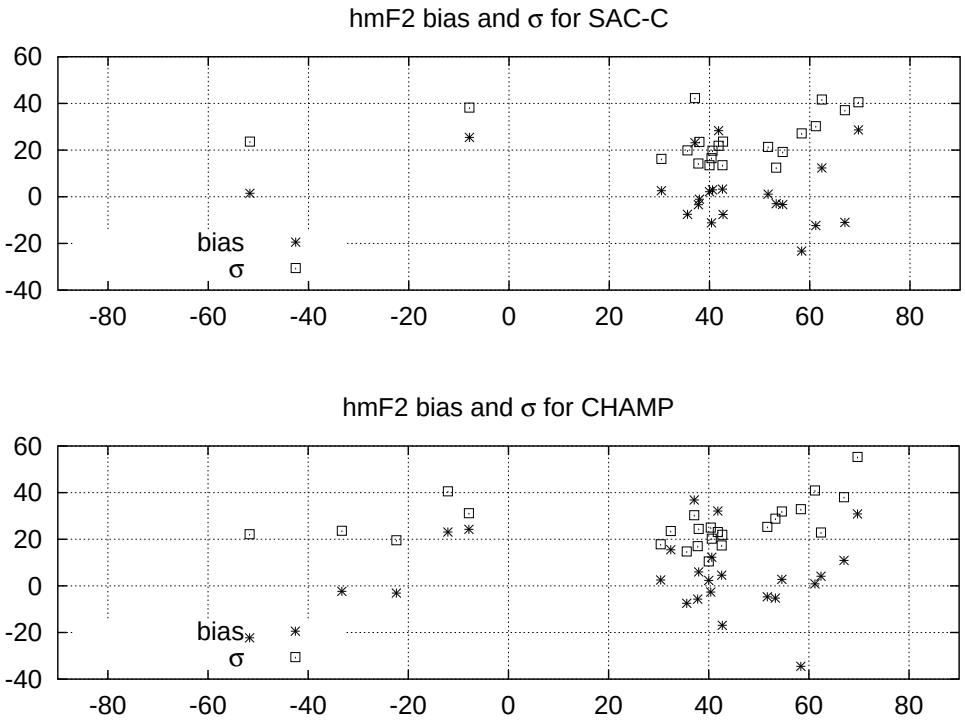

Figure 6.19: This plot depicts the latitude dependency of the hmF2 parameter for the both the SAC-C and CHAMP satellites during the period studied, which runs from 2002 November 1st to 2002 November 16th..

6.6.3 Upper Ionosphere and Plasmasphere estimation

As mentioned before, this issue is critical for satellites at very low orbits such as CHAMP. As in the case of the GPSMET satellite, the contribution of the electron content above the LEO orbit is taken into account by the variable F_p to estimate in the process. In the upper panel of Figure 6.20, the plasmaspheric estimations for the SAC-C and CHAMP satellites are depicted. Note that, as expected, the estimation for the CHAMP satellite is higher than the SAC-C since the lower the orbit, the higher the electron content above the LEO. To assess the validity of this approach, it is given in the lower panel the same result using a voxel model approach (where only all POD data with an elevation mask of 10^o has been used to obtain the density above the LEO). In both cases, no aprioris have been used.

The comparison with the voxel model shows certain agreement between the two approaches, which indicates a reasonable estimation of the upper ionosphere and plasmasphere despite that the shape function above the LEO

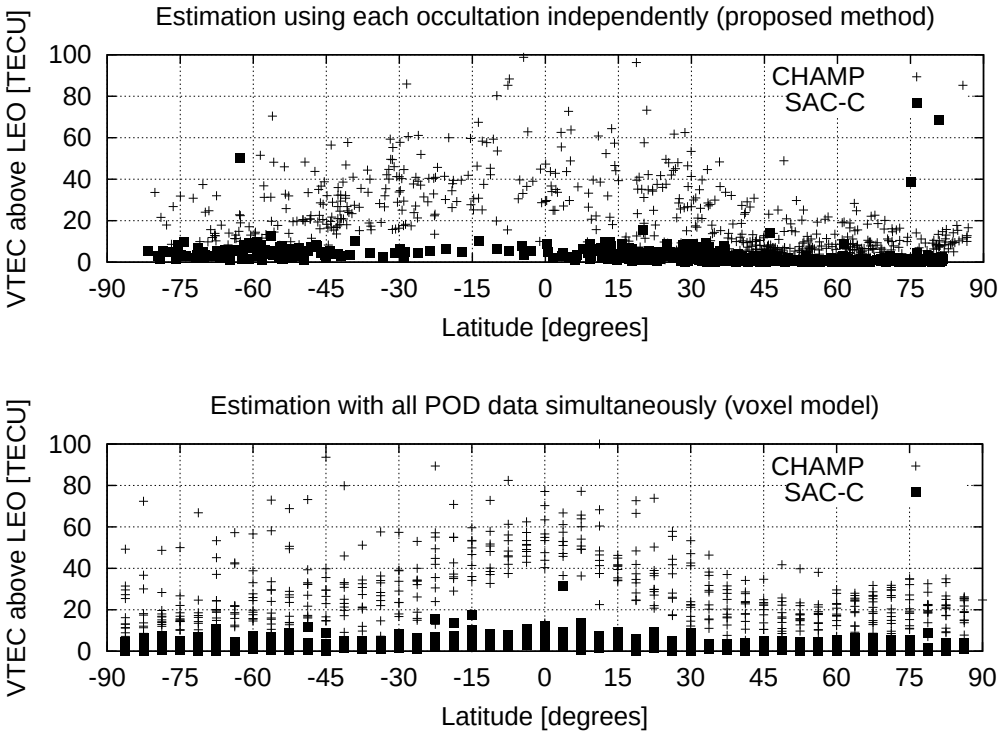

Figure 6.20: Upper ionosphere and plasmaspheric estimation for SAC-C and CHAMP satellites. The estimation corresponds to the scenario that runs from 2002 November 1st to 2002 November 16th. Upper panel shows the estimations corresponding to each occultation processed independently. Lower panel shows the estimation using the voxel model and all positive elevation data (POD).

has been estimated for each occultation processed independently. Since this estimation affects the rest of the profile, this statement is supported by the comparison with ionosonde parameters, where differences between spherical symmetry and separability hypothesis are partially due to how well the electron content above the LEO is estimated.

6.6.4 Intercomparison between SAC-C and CHAMP

Since SAC-C and CHAMP satellites are currently gathering information at the same time, it is possible to search for spatial and temporal coincident occultation events between CHAMP and SAC-C (i.e. co-located occultations) and compare profiles between them.

In this context, two types of comparisons are made, the discrepancies in the peak values and the peak height values. To compare the results with previous sections, figures are provided in frequency units. In the case of spherical symmetry the profile is directly electron density, therefore, expression 1.24 is used. In the case of separability, the profile is given in units of shape function $[m^{-1}]$, which is linked to electron density through the VTEC. Although the shape function does not have a direct physical meaning as frequency or electron density, the table provides with the bias and σ for this shape function intercomparison. To relate these discrepancies to previous figures of frequency comparison, the relative (percentual) RMS differences are given as well, to compute this relative RMS, the square root is applied to the shape function in order to transform its units to a frequency-like ones. The profiles of the SAC-C satellite are the chosen reference for this comparison.

Day period		Separability hypothesis			Spherical symmetry		
	# comp.	bias $[10^{-6}\ m^{-1}]$	σ	Rel. RMS [%]	bias [MHz]	σ	Rel. RMS [%]
Day	283	-0.2	0.9	14.4	-0.2	1.8	18.7
D & D	27	0.1	1.3	23.8	-1.0	1.9	38.9
Night	207	-0.1	1.2	24.1	-1.0	3.2	54.3

Table 6.10: Shape Function peak inter-comparison for the SAC-C and CHAMP satellites.

The results of this table show that the discrepancies are consistent with the comparison with ionosondes, that is, the results with spherical symmetry are improved with the proposed approach of separability.

Additionally, it is possible to obtain a F2 layer peak height inter-comparison between the co-located profiles of both satellites. The results are summarized in Table 6.11, where a similar performance with respect to the comparison of the hmF2 computed with Dudeney applied to ionosonde data is stated. The differences are kept approximately to 30km.

As an "*a posteriori*" justification of the goodness of using shape function, the case study of the situation depicted in Figure 6.21 is given. The map shows several profiles of either CHAMP and SAC-C satellite co-located in the region of South America. The VTEC gradients are also shown, note that since the Equatorial Anomalies are present, the variation of VTEC can reach values larger than 50TECU. The corresponding profiles of this occultation can be viewed in Figure 6.22 using the same color coding.

Note how the electron density profiles (computed with spherical symmetry) follow the VTEC behavior (the larger the VTEC the larger the electron density). It can be seen that there are differences in the shape of the profile

Day period	Separability hypothesis			Spherical symmetry		
	# comp.	bias	σ [km]	# comp.	bias	σ [km]
Daytime	255	-2.8	28.0	197	-2.2	31.7
Dawn & Dusk	25	-7.7	32.2	22	-16	32.8
Nighttime	180	-4.4	38.2	148	-9.9	48.6

Table 6.11: Shape Function peak height inter-comparison for the SAC-C and CHAMP satellites for the period that runs from 2002 November 1st to 2002 November 16th. The number of comparison is different because it has been imposed a filter that the hmF2 is placed between 200km and 400km

(left panel, Figure 6.22). Nevertheless if shape functions (F) are computed instead (using the separability approach, right panel, Figure 6.22), the shapes are closer. This means that the horizontal variation of shape functions is lower than electron density ones. Note that this property is true for the VTEC scaling (that accounts for horizontal gradients), but there are almost no effect on the true height scale. A possible solution to this issue could be the use of more than one shape function in order to take into account this height variability.

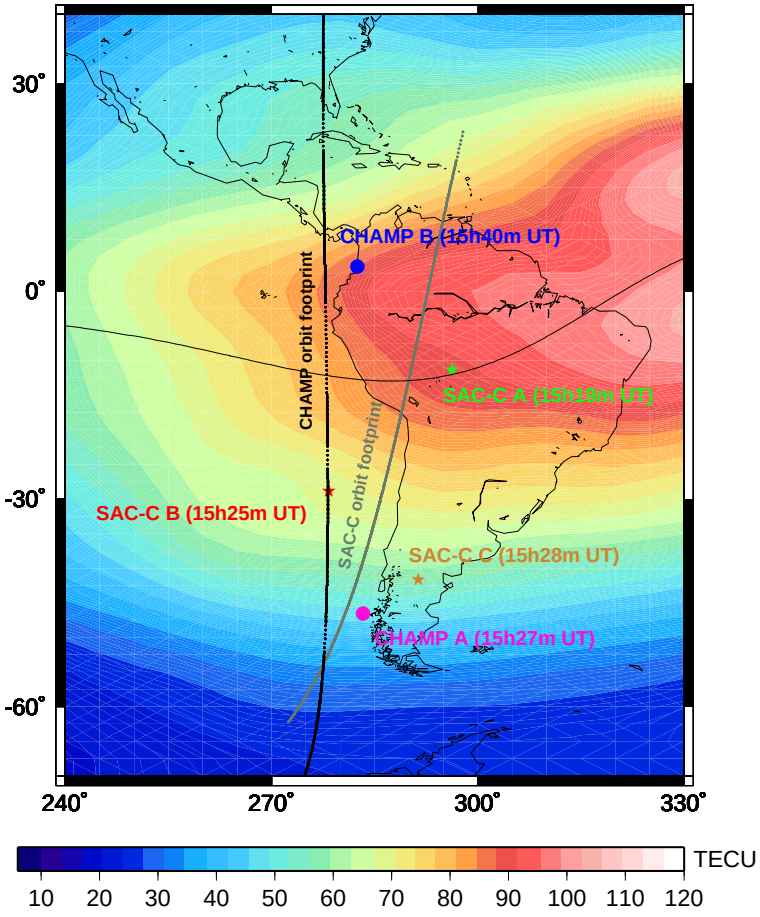

Figure 6.21: Co-located profiles of SAC-C and CHAMP in South America. During the occultations (that took place in 2002 November 3rd) high VTEC gradients were experienced (15hUT, 10hLT approximately). Stars and circles indicate the location of the SAC-C and CHAMP occultations respectively. The corresponding orbit footprints are also depicted.

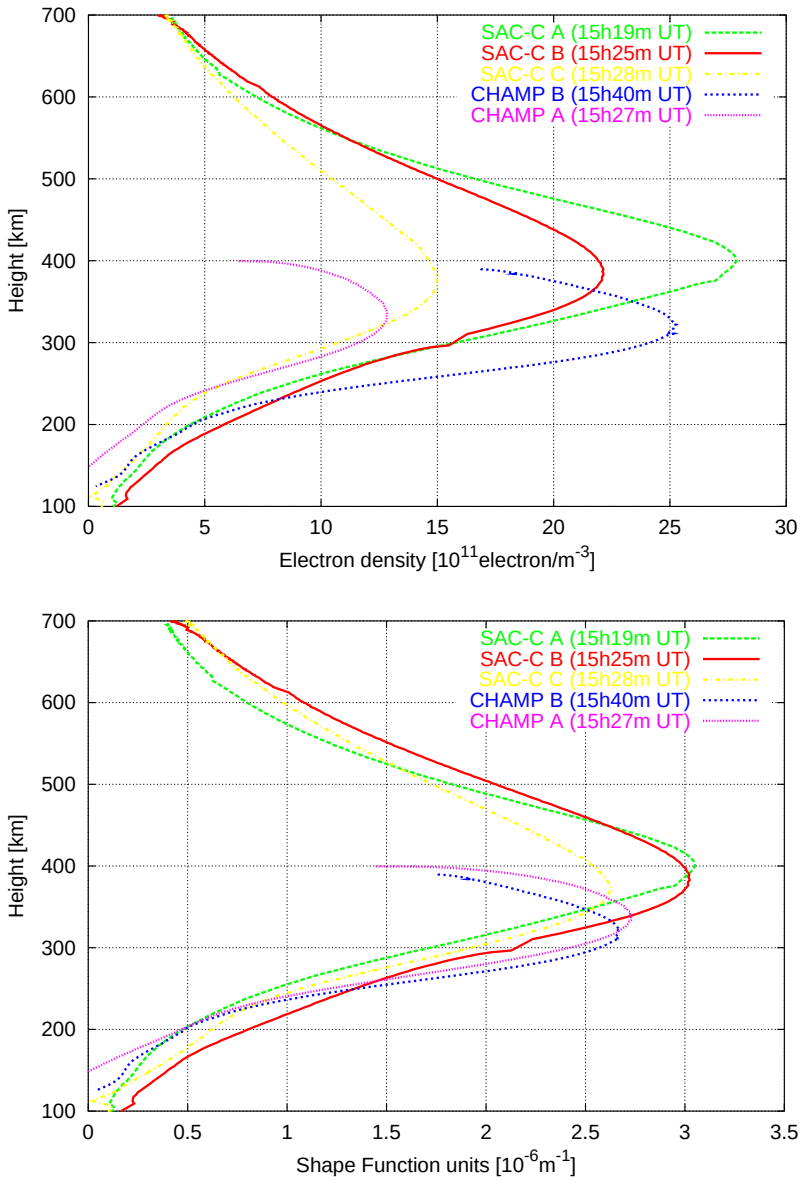

Figure 6.22: Co-located vertical profiles of SAC-C and CHAMP in South America

Conclusions and guidelines for future research

Conclusions

This doctoral thesis proposes the study and development of two techniques in the context of ionospheric tomography based with GPS data:

1. It has been shown how the *combination of data* of different nature can provide with benefits related to the vertical description of the ionosphere.

2. It has been shown an *improved Abel transform* algorithm that uses VTEC data to improve the classical scheme of Abel inversion assuming spherical symmetry.

Conclusions and key points of both issues are discussed in the following sections.

Combination of data

In Chapter 5 it was shown the feasibility of data combination in a data driven model between GPS ground data and vertical profiles of electron density computed from ionosonde data. The performance of this technique was shown through two scenarios: (1) reconstruction of N_e profiles (i.e. comparison with ionosondes) and (2) reconstruction of STEC observations (i.e. comparison with GPSMET observations).

In the first scenario, the vertical profiles of electron density where reconstructed using all ground GPS data and vertical profiles derived from one or two ionosondes. From the results of comparison with test ionosondes that did not take part into the process, the performances in the estimation of the maximum of electron density during low geomagnetic activity are in general better than 20% (note that the average performance of classical Abel inversion is between 20% and 40% in electron density). An additional feature of

this technique is that valuable information about topside ionosphere can be obtained using constraints based on ratios extracted from a model.

In a second scenario, the STEC observations seen by the GPS/MET were reconstructed using all GPS data and ionosonde derived profiles. The results reported a good agreement between these reconstructed profiles with the actual measurements. In fact, the discrepancy was less than 25% for STEC observations with height of impact parameter below hmF2. Therefore, this approach showed that it is possible to model GPS LEO observations with only ground GPS and ionosonde data, specially below the electron density peak.

Summarizing, the proposed technique of data combination showed the possibility of obtaining vertical information of electron density in locations where no ionosonde was present. That is, thanks to the combination of GPS and ionosonde data, an expansion of the vertical information of the ionosonde can be obtained.

Improved Abel transform

As developed in Chapter 6, in order to overcome the limitation of the classical Abel inversion (i.e. spherical symmetry), the algorithm was modified to include information of the horizontal variability of the electron density. This information can be given by the VTEC due to the potential proportionality between the VTEC and the electron density (stated by a constant value of slab thickness in the case of the F2 layer peak). The approach introduced the concept of shape functions, which are the unknowns to be solved by this algorithm and act as a vertical descriptor of the electron density. Therefore a *separability* between these shape functions and VTEC was stated.

This modification of the Abel inversion leads to an improvement in the foF2 and foE estimation by an average value of 30% or even more when a comparison with ionosonde parameters are performed. This improvement is verified in different latitudes, local times, different ionospheric conditions, solar cycle and data sets from different satellites.

Since the correlation radii of the shape function are larger than the electron density profiles, the error due to the spatial/temporal mismatch between the ionosonde and occultation (i.e. co-location error) is diminished. Here, the VTEC data informs about the spatial/temporal variability of the electron density.

With respect to the discrepancies of the true height estimation of hmF2 with Dudeney or POLAN, in the case of GPSMET it was stated a standard deviation of 25km approximately with a certain dependence on latitude (worsen results for ionosondes close to equator), similar results were experi-

enced with other data sets gathered by SAC-C and CHAMP satellites. This latitude dependency is explained by the fact that a single shape function is not able to perform a complete description of the height variations of the profile. Note that the shape function of an occultation is scaled in frequency using the VTEC, but this does not modify the height axis of the profile. Similarly to previous authors, depending on the ratio $foF2/FoE$, the bias of this discrepancy showed a certain variability. Results show that similar performance regarding the discrepancies with respect to Dudeney formula (less than 30km) can be obtained regardless the satellite used.

An additional feature of the proposed improvement of the Abel technique is the treatment of the upper ionosphere and plasmasphere. In the method an additional unknown was included in order to account for the electron content above the LEO. The estimation obtained with each occultation could be compared with a tomographic voxel model, showing good agreement, taking into account that the shape function value above the LEO is estimated using only one occultation. Although being at different heights, the comparisons of different ionospheric parameters indicate that the proposed method of estimating the upper ionosphere and plasmasphere is valid in either satellites at very low orbits such as CHAMP and higher orbits such as GPSMET or SAC-C.

Guidelines for future research

Possible improvements of the techniques described in this work start with the idea of a separability expansion, that is, not only considering separability at the level of a VTEC function and a single shape function but several shape functions as well. That is, to invert an occultation based on more than one shape function. In order to avoid under-determination of the system of equations (less data than unknowns), the joint process of more than one radio occultation are needed in order to perform this (in fact, at least equal number of occultations and profiles). With this approach, the observations of each radio occultation will improve the overall estimation.

This idea constitutes the backbone of a more ambitious guideline. To establish a starting point of this technique, a summary of pros and cons of both methods used in this thesis work (tomography based on 3D voxels and classical Abel transform) is given:

	Abel transform	3D Voxels
Vertical resolution	$\approx$ **1 km**	10 $\sim$ 100 km
Computational load	**Low ($\simeq 10^2$ unk.)**	High ($\geq 10^3$ unk.)
Spherical Symmetry assumption	Yes	**No**
Topside mismodelling	Yes	**No**
Combination capability	No	**Yes**

Following the main idea of combination in order to compensate the drawbacks of one technique with the strong points of the other, it seems feasible that a technique that considers both approaches at the same time may result in an overall improvement of ionospheric tomography. The main idea is to use the concept of shape functions instead of electron densities as the unknown to solve. As mentioned in previous sections, the correlation radii of the shape functions are larger, thus allowing a reduction of the number of variables in the horizontal dimension. The VTEC, that would be computed by another process, would account for the horizontal variability of the electron density. Therefore considering a limited set of shape functions (definitely less in number than electron density profiles), it would be possible to obtain a global description of the ionosphere.

A limitation of this technique is the sparsity of data. Although the number of GPS ground receivers has been increased in the recent years, it remains the main issue of the coverage in regions with lack of receivers (mainly oceans and seas). This can be partially overcome using interpolation, climatological models and with data from LEO GPS receivers. Moreover, the coverage of these satellite receivers is not global. With the advent of the COSMIC satellite and the joint process of data from different satellites, in near future this issue will be fulfilled.

Future implementations of this technique may be related to near real-time or even real-time capabilities. Currently the technology to obtain global VTEC maps in real time is at hand and there is an initiative of IGS to provide with data from GPS stations in real time. The next step to these VTEC maps, when the techniques are improved and refined, could be the implementation with shape functions in order to obtain a global 3D description of the ionosphere in real-time.

APPENDIX A: Acronyms

AS	Anti/Spoofing
CHAMP	CHAllenging Minisatellite Payload
CME	Coronal Mass Ejection
EOF	Empirical Orthogonal Functions
GIM	Global Ionospheric Map
GNSS	Global Navigation Satellite System
GOLPE	GPS OccuLtation and Passive reflection Experiment
GPS	Global Positioning System
GPSMET	GPS/METeorology
IGS	International GPS Service
IONEX	IONosphere Map EXchange
IRI	International Reference Ionosphere
ISR	Incoherent Scatter Radar
LEO	Low Earth Orbiter
LMS	Least Mean Square
PLP	Planar Langmuir Probe
POD	Precise Orbit Determination
RMS	Root Mean Square
SA	Selective Availabilty
SAC-C	Satelite de Aplicaciones Cientificas
STEC	Slant Total Electron Content
TEC	Total Electron Content
TID	Traveling Ionospheric Disturbances
UPC	Universitat Politècnica de Catalunya
UT	Universal Time
VTEC	Vertical Total Electron Content
WLMS	Weighted Least Mean Square

Bibliography

[Austen et al., 1988] Austen, J. R., Franke, S. J. and Liu, C., 1988. Ionospheric imaging using computerized tomography. Radio Science 23(3), pp. 299–307.

[Bierman, 1977] Bierman, G. J., 1977. Factorization Methods for Discrete Sequential Estimation. Mathematics in Science and Engineering, Vol. 128, Academic Press.

[Bilitza, 1990] Bilitza, D., 1990. International reference ionosphere 1990. URSI/COSPAR, NSSDC/WDC-A-R&S 90-22.

[Bilitza, 2001] Bilitza, D., 2001. International reference ionosphere 2000. Radio Science 36(2), pp. 261.

[Bilitza et al., 1979] Bilitza, D., Sheikh, N. and Eyfrig, R., 1979. A global model for the height of the F2-peak using M3000 values from the CCIR numerical map. Telecomunications Journal (46), pp. 549–553.

[Blewitt, 1989] Blewitt, G., 1989. Carrier Phase Ambiguity Resolution for the Global Positioning System Applied to Geodetic Baselines up to 2000km. Journal of Geophysical Research 94, pp. 10187–10203.

[Born and Wolf, 1975] Born, M. and Wolf, E., 1975. Principles of Optics: Electromagnetic Theory of Propagation, Interference and Diffraction of Light. Pergamon Press.

[Bracewell, 2000] Bracewell, R., 2000. The Fourier Transform and its applications. McGraw-Hill Higher Education.

[Bradley and Dudeney, 1973] Bradley, P. and Dudeney, J., 1973. A simple model of the vertical distribution of the electron concentration in the ionosphere. Journal of Atmospheric Terrestrial Physics (35), pp. 2131–2146.

[Breed and Goodwin, 1998] Breed, A. and Goodwin, G., 1998. Ionospheric slab thickness and total electron content determined in Australia.

[Brekke, 1997] Brekke, A., 1997. Physics of the upper polar atmosphere. Wiley-Praxis Series in Atmospheric Physics, John Wiley & Sons.

[Davies, 1990] Davies, K., 1990. Ionospheric Radio. Institution of Electrical Engineers, London, United Kingdom.

[Dudeney, 1983] Dudeney, J., 1983. The accuracy of simple methods for determining the height of the maximum electron concentration of the F2 layer from scaled ionospheric characteristics. Journal of Atmospheric Terrestrial Physics (45), pp. 629.

[Feltens and Schaer, 1998] Feltens, J. and Schaer, S., 1998. IGS products for the ionosphere. Proceedings of the IGS Analysis Center Workshop, ESA/ESOC.

[Fremouw et al., 1992] Fremouw, E., Secan, J. A. and Howe, B. M., 1992. Application of stochastic inverse theory to ionospheric tomography. Radio Science.

[Garcia-Fernandez et al., 2003a] Garcia-Fernandez, M., Hernandez-Pajares, M., Juan, M. and Sanz, J., 2003a. Improvement of ionospheric electron density estimation with GPSMET occultation using Abel inversion and VTEC information. Journal of Geophysical Research - Space Physics 108, pp. 1338.

[Garcia-Fernandez et al., 2003b] Garcia-Fernandez, M., Hernandez-Pajares, M., Juan, M. and Sanz, J., 2003b. An improvement of retrieval techniques for ionospheric radio occultations. In: First CHAMP Mission Results, for Gravity, Magnetic and Atmospheric Studies, Springer, Germany, pp. 430–440.

[Garcia-Fernandez et al., 2002] Garcia-Fernandez, M., Hernandez-Pajares, M., Juan, M., Sanz, J. and Orus, R., 2002. Ionospheric data combination as a way to improve electron density estimations. Acta Geodetica Geophisica Hungarica 37(2-3), pp. 203–211.

[Garcia-Fernandez et al., 2003c] Garcia-Fernandez, M., Hernandez-Pajares, M., Juan, M., Sanz, J., Orus, R., Coisson, P., Nava, B. and Radicella, S. M., 2003c. Combining ionosonde with ground GPS data for electron density estimation. Journal of Atmospheric and Solar-Terrestrial Physics 65, pp. 683–691.

[Hajj et al., 2000] Hajj, G. A., Lee, L. C., Pi, X., Romans, L. J., Schreiner, W. S., Straus, P. R. and Wang, C., 2000. COSMIC GPS Ionospheric Sensing and Space Weather. TAO 11(1), pp. 235–272.

[Hajj et al., 2002] Hajj, G. A., Wilson, B. D., Wang, C., Pi, X. and Rosen, I. G., 2002. Ionospheric Data Assimilation of Ground GPS TEC by Use of the Kalman Filter. Submitted to Radio Science.

[Hajj and Romans, 1998] Hajj, G. and Romans, L., 1998. Ionospheric electron density profiles obtained with the Global Positioning System: Results from the GPS/MET experiment. Radio Science 33(1), pp. 175–190.

[Hajj et al., 1994] Hajj, G., Ibañez-Meier, R., Kursinski, E. and Romans, L., 1994. Imaging the Ionosphere with the Global Positioning System. International Journal of Imaging Systems and Technology 5, pp. 174–184.

[Hardy et al., 1993] Hardy, K., Hajj, G. A., Kursinski, E. and Ibáñez-Meier, R., 1993. Accuracies of atmospheric profiles obtained from GPS occultations. Proceedings of the ION GPS-93 Conference pp. 1545–1556.

[Hernandez-Pajares et al., 1998] Hernandez-Pajares, M., Juan, M. and Sanz, J., 1998. Global observation of the ionospheric electronic response to solar events using ground and LEO GPS data. Journal of Geophysical Research (Space Physics) 103(9), pp. 20789–20796.

[Hernandez-Pajares et al., 1999] Hernandez-Pajares, M., Juan, M. and Sanz, J., 1999. New approaches in global ionospheric determination using ground GPS data. Journal of Atmospheric and Solar-Terrestrial Physics 61, pp. 1237–1247.

[Hernandez-Pajares et al., 2000] Hernandez-Pajares, M., Juan, M. and Sanz, J., 2000. Improving the Abel inversion by adding ground data LEO radio occultations in the ionospheric sounding. Geophysical Research Letters 27(16), pp. 2743–2746.

[Hernandez-Pajares et al., 2002] Hernandez-Pajares, M., Juan, M., Sanz, J. and Bilitza, D., 2002. Combining GPS measurements and IRI model values for space weather specification. Advances in Space Research 29(6), pp. 949–958.

[Hochegger et al., 2000] Hochegger, G., Nava, B., Radicella, S. and Leitinger, R., 2000. A Family of Ionospheric Models for Different Uses. Phys. Chem. Earth 25(4), pp. 307–310.

[Hoffmann-Wellenhof et al., 1994] Hoffmann-Wellenhof, B., Lichtenegger, H. and Collins, J., 1994. GPS: Theory and Practice. Springer-Verlag, Wien, New York.

[Howe et al., 1998] Howe, B. M., Runciman, K. and Secan, J., 1998. Tomography of the ionosphere: Four-dimensional simulations. Radio Science 33(1), pp. 109.

[Jakowski et al., 2003] Jakowski, N., Wehrenpfennig, A., Heise, S., Reigber, C. and Lühr, H., 2003. Status of Ionospheric Radio Occultation CHAMP Data Analysis and Validation of Higher Level Data Products. pp. 462–472.

[Jakowski et al., 2002] Jakowski, N., Wehrenpfennig, A., Heise, S., Reigber, C., Lühr, H., Grunwaldt, L. and Meehan, T., 2002. GPS radio occultation measurements of the ionosphere from CHAMP: Early results.

[Kak and Slaney, 1988] Kak, A. and Slaney, M., 1988. Principles of Computerized Tomographic Imaging. IEEE Press.

[Koch, 1988] Koch, K., 1988. Parameter Estimation and Hypothesis Testing in Linear Models. Springer-Verlag, Berlin, Germany.

[Komjathy and Hernandez-Pajares, 2004] Komjathy, A. and Hernandez-Pajares, M., 2004. The IGS Global TEC maps: Present and Future. 2004 National Radio Science Meeting, Boulder, CO, USA.

[Leitinger, 1994] Leitinger, R., 1994. Data from Orbiting Navigation Satellites for Tomographic Reconstruction. International Journal of Imaging Systems and Technology 5(2), pp. 86–96.

[Leitinger et al., 1997] Leitinger, R., Ladreiter, H. and Kirchengast, G., 1997. Ionosphere tomography with data from satellite reception of Global Navigation Satellite Systems signals and ground reception of Navy Navigation Satellite System signals. Radio Science 32(4), pp. 1657–1669.

[Marin et al., 2001] Marin, D., Mikhailov, A., Morena, B. d. l. and Herraiz, M., 2001. Long-term hmF2 trends in the Eurasian longitudinal sector from the ground-based ionosonde observations. Annales Geophysicae (19), pp. 761–772.

[McNamara et al., 1987] McNamara, L., Reinisch, B. and Tang, J., 1987. Values of hmF2 deduced from automatically scaled ionograms. Advances in Space Research 7(6), pp. (6)53–(6)56.

[O'Loughlin, 1997] O'Loughlin, K. F., 1997. SPIDR on the Web: Space Physics Interactive Data Resource on-line analysis tool. Radio Science 32(5), pp. 2021.

[Orus et al., 2002] Orus, R., Hernandez-Pajares, M., Juan, M., Sanz, J. and Garcia-Fernandez, M., 2002. Performance of different TEC models to provide GPS ionospheric corrections. Journal of Atmospheric and Solar-Terrestrial Physics 64, pp. 2055–2062.

[Orus et al., 2003] Orus, R., Hernandez-Pajares, M., Juan, M., Sanz, J. and Garcia-Fernandez, M., 2003. Validation of the GPS TEC maps with TOPEX data. Advances in Space Research 31(3), pp. 621–627.

[Parkinson and Spilker Jr., 1996] Parkinson, B. W. and Spilker Jr., J. J., 1996. Global Positioning System: Theory and Applications. Volumes I & II. American Institute for Aeronautics and Astronautics, Inc.

[Piggot and Rawer, 1978] Piggot, W. and Rawer, K., 1978. URSI Handbook of ionogram interpretation and reduction. World Data Center A for Solar-Terrestrial Physics.

[Raymund et al., 1990] Raymund, T., Austen, J., Liu, C., Klobuchar, J. and Stalker, J., 1990. Application of computerized tomography to the investigation of ionospheric structures. Radio Science 25(5), pp. 771–789.

[Raymund et al., 1994] Raymund, T., Bresler, Y., Anderson, D. and Daniell, R., 1994. Model-assisted ionospheric tomography: A new algorithm. Radio Science 29(6), pp. 1493–1512.

[Rishbeth et al., 2000] Rishbeth, H., Sedgemore-Schulthess, K. and Ulich, T., 2000. Semiannual and annual variations in the height of the ionospheric F2-peak. Ann. Geophysicae (18), pp. 285–299.

[Sardon et al., 1994] Sardon, E., Rius, A. and Zarraoa, N., 1994. Estimation of the transmitter and receiver differential biases and the ionospheric total electron content from Global Positioning System observations. Radio Science 29(3), pp. 577–586.

[Schaer et al., 1998] Schaer, S., Gurtner, W. and Feltens, J., 1998. IONEX: The IONosphere map Exchange. Format Version 1. Proceedings of the IGS AC Workshop.

[Schreiner et al., 1999] Schreiner, W., Sokolovskiy, S., Rocken, C. and Hunt, D., 1999. Analysis and validation of GPS/MET radio occultation data in the ionosphere. Radio Science 34(4), pp. 949–966.

[Seeber, 1992] Seeber, G., 1992. Satellite Geodesy. Walter de Gruyter, Inc.

[Shimazaki, 1955] Shimazaki, T., 1955. World-wide variations in the height of the maximum electron density of the ionospheric F2 layer. Journal Radio Research Laboratory 7(2), pp. 85–97.

[Sutton and Na, 1996] Sutton, E. and Na, H., 1996. A Block Iterative Algorithm for Tomographic Reconstruction of Ionospheric Electron Density. International Journal of Imaging Systems and Technology 7(3), pp. 238–245.

[Titheridge, 1998] Titheridge, J., 1998. The real height analysis of ionograms: A generalized formulation. Radio Science 23(5), pp. 831–849.

[Tricomi, 1985] Tricomi, G., 1985. Integral Equations. Dover Publications, New York.

[Tsai et al., 2001] Tsai, L., Tsai, W., Schreiner, W., Berkey, F. and Liu, J., 2001. Comparisons of GPS/MET retrieved ionospheric electron density and ground based ionosonde data. Earth Planets Space 53, pp. 193–205.

[Welch and Bishop, 2003] Welch, G. and Bishop, G., 2003. The Kalman Filter, http://www.cs.unc.edu/∼welch/kalman/.

[Wells, 1987] Wells, D., 1987. Guide to GPS positioning. Canadian GPS associates, Frederickton.

[World Data Center-A, 2003] World Data Center-A, 2003. Rutherford Appleton Laboratory, http://www.wdc.rl.ac.uk.

[Yeh and Raymund, 1991] Yeh, K. and Raymund, T., 1991. Limitations of ionospheric imaging by tomography. Radio Science 26, pp. 1361–1380.

[Zhang et al., 1999] Zhang, S., Fukao, S., Oliver, W. and Otsuka, Y., 1999. The height of the maximum ionospheric electron density over the MU radar. Journal of Atmospheric and Solar-Terrestrial Physics 61, pp. 1367–1383.